Calhoun: The NPS Institutional Archive

DSpace Repository

Theses and Dissertations | 1. Thesis and Dissertation Collection, all items

1990-09

Flow modification over a backward facing step

Narveson, Marshall L.

Monterey, California: Naval Postgraduate School

http://hdl.handle.net/10945/34915

This publication is a work of the U.S. Government as defined in Title 17, United States Code, Section 101. Copyright protection is not available for this work in the United States.

Downloaded from NPS Archive: Calhoun

http://www.nps.edu/library

Calhoun is the Naval Postgraduate School's public access digital repository for research materials and institutional publications created by the NPS community. Calhoun is named for Professor of Mathematics Guy K. Calhoun, NPS's first appointed -- and published -- scholarly author.

Dudley Knox Library / Naval Postgraduate School
411 Dyer Road / 1 University Circle
Monterey, California USA 93943

NAVAL POSTGRADUATE SCHOOL
Monterey, California

AD-A241 351

DTIC
ELECTE
OCT 0 8 1991
S B D

THESIS

FLOW MODIFICATION OVER
A
BACKWARD FACING STEP

by

Marshall L. Narveson

September, 1990

Thesis Advisor: J. Val Healey

Approved for public release; distribution is unlimited.

91-12537

Unclassified

Security Classification of this page

REPORT DOCUMENTATION PAGE

1a Report Security Classification: Unclassified	1b Restrictive Markings
2a Security Classification Authority	3 Distribution Availability of Report: Approved for public release; distribution is unlimited.
2b Declassification/Downgrading Schedule	
4 Performing Organization Report Number(s)	5 Monitoring Organization Report Number(s)
6a Name of Performing Organization: Naval Postgraduate School; 6b Office Symbol (If Applicable): AA/HE	7a Name of Monitoring Organization: Naval Postgraduate School
6c Address (city, state, and ZIP code): Monterey, CA 93943-5000	7b Address (city, state, and ZIP code): Monterey, CA 93943-5000
8a Name of Funding/Sponsoring Organization; 8b Office Symbol (If Applicable)	9 Procurement Instrument Identification Number
8c Address (city, state, and ZIP code)	10 Source of Funding Numbers: Program Element Number; Project No; Task No; Work Unit Accession No

11 Title (Include Security Classification): FLOW MODIFICATION OVER A BACKWARD FACING STEP

12 Personal Author(s): Marshall L. Narveson

13a Type of Report	13b Time Covered	14 Date of Report (year, month,day)	15 Page Count
Master's Thesis	From To	September 1990	100

16 Supplementary Notation: The views expressed in this thesis are those of the author and do not reflect the official policy or position of the Department of Defense or the U.S. Government.

17 Cosati Codes			18 Subject Terms (continue on reverse if necessary and identify by block number)
Field	Group	Subgroup	Backward Facing Step, Flow Visualization, Bluff Body Aerodynamics, Helium Bubble Flow Visualization, Deflectors, Flow Modification

19 Abstract (continue on reverse if necessary and identify by block number)

The Naval Postgraduate School (NPS) has undertaken a series of studies on ship air wake tailoring, through the use of deflectors, with the goal of reducing the level of turbulence and the size of the separated zones on the helicopter deck. This reduction will result in a larger engage/disengage envelope, which in turn, will increase the percentage of time that the H-46 and other helicopters can safely operate. This study is the second in the series at NPS to attempt to achieve this goal and considers only the feasibility of tailoring a two-dimensional flow over a backward facing step. Nonporous flat and curved deflectors and porous flat deflectors were mounted in various positions near the edge of the step and the flow patterns recorded using both still and video photography. The deflectors were mounted at varying separations from the step and varying angles to the vertical. It was found that the porous deflectors produced the lowest velocities in the region behind the step, and the nonporous produced the greatest changes in the flow pattern. The results were also compared to the results of the first study that used the "PHOENICS" computational fluid dynamics program. With one exception, the results differed only by the underprediction of the length of the horizontal flow pattern.

20 Distribution/Availability of Abstract	21 Abstract Security Classification	
[X] unclassified/unlimited [ ] same as report [ ] DTIC users	Unclassified	
22a Name of Responsible Individual: J. Val Healey	22b Telephone (Include Area code): (408) 646-2804	22c Office Symbol: AA/HE

DD FORM 1473, 84 MAR — 83 APR edition may be used until exhausted — All other editions are obsolete

security classification of this page: Unclassified

Approved for public release; distribution is unlimited.

Flow Modification Over a Backward
Facing Step

by

Marshall L. Narveson
Lieutenant Commander, United States Navy
B.S., University of Wisconsin-Madison, 1978

Submitted in partial fulfillment
of the requirements for the degree of

MASTER OF SCIENCE IN AERONAUTICAL ENGINEERING

from the

NAVAL POSTGRADUATE SCHOOL
September, 1990

Author: [redacted]
Marshall L. Narveson

Approved by: [redacted]
J. Val Healey, Thesis Advisor

[redacted]
Richard M. Howard, Second Reader

[redacted]
E. Roberts Wood, Chairman
Department of Aeronautics and Astronautics

ABSTRACT

The Naval Postgraduate School (NPS) has undertaken a series of studies on ship air wake tailoring, through the use of deflectors, with the goal of reducing the level of turbulence and the size of the separated zones on the helicopter deck. This reduction will result in a larger engage/disengage envelope, which in turn, will increase the percentage of time that the H-46 and other helicopters can safely operate. This study is the second in the series at NPS to attempt to achieve this goal and considers only the feasibility of tailoring a two-dimensional flow over a backward facing step. Nonporous flat and curved deflectors and porous flat deflectors were mounted in various positions near the edge of the step and the flow patterns recorded using both still and video photography. The deflectors were mounted at varying separations from the step and varying angles to the vertical. It was found that the porous deflectors produced the lowest velocities in the region behind the step, and the nonporous produced the greatest changes in the flow pattern. The results were also compared to the results of the first study that used the "PHOENICS" computational fluid dynamics program. With one exception, the results differed only by the underprediction of the length of the horizontal flow pattern.

Accession For	
NTIS GRA&I	☑
DTIC TAB	☐
Unannounced	☐
Justification	
By	
Distribution/	
Availability Codes	
Dist	Avail and/or Special
A-1	

ACKNOWLEDGEMENTS

I wish to express my sincere appreciation to all the people that made it possible for me to complete this project. I would particularly like to thank Professor Healey for his support and Ron Ramaker and John Moulton for their fine workmanship in constructing the needed equipment in a timely fashion. I also would like to thank the personnel in the Photo Lab for their outstanding last minute effort to develop, print and make half-tones of several hundred photos. I reserve my deepest gratitude for my wife, Janice, without whose support this project would have been impossible for me to complete. She supported me both emotionally and in terms of the extra work load she carried on my behalf.

Above all, I want to express my thanks to God. The ability to think clearly and work with determination are gifts from Him, for what does a man have that God has not given him.

TABLE OF CONTENTS

I. INTRODUCTION 1

II. BACKGROUND 4

A. HELICOPTER OPERATIONS 4

B. BLUFF BODY AERODYNAMICS 9

C. FLOW OVER A BACKWARD FACING STEP 14

D. FLOW OVER A TWO-DIMENSIONAL OBSTACLE 18

E. FLOW MODIFICATION 20

III. EXPERIMENTAL APPARATUS 24

A. WIND TUNNEL 24

B. THE STEP 26

C. THE DEFLECTORS 28

D. HOT WIRE ANEMOMETER 29

E. THE CONSTANT TEMPERATURE ANEMOMETER UNIT AND BRIDGE 29

F. THE ANALOG TO DIGITAL CONVERTER 30

G. THE COMPUTER 30
H. ACQUISITION AND PROCESSING SOFTWARE 31
I. HELIUM BUBBLE GENERATION 31
J. LIGHTING 32
K. STILL PHOTOGRAPHY 32
L. VIDEO 32

IV. EXPERIMENTAL PROCEDURE 33
A. TUNNEL CALIBRATION 33
B. FLOW VISUALIZATION 35
1. Deflector Placement 35
2. Helium Bubbles 37
C. HOT WIRE ANEMOMETRY 37

V. RESULTS AND DISCUSSION 39
A. VALIDATION OF "PHOENICS" CFD RESULTS 39
B. FLAT NON-POROUS DEFLECTORS 47
1. Vertical Deflectors 47
2. 30 Degree Deflectors 47
3. 45 Degree Deflectors 51
4. Summary 53

C. FLAT POROUS DEFLECTORS 54
1. Vertical Deflectors 54
2. 30 Degree deflectors 59
3. 45 Degree Deflectors 63
4. Negative-Angle Deflectors 63
5. Summary 64
D. CURVED DEFLECTORS 66
1. 90 Degree Arc Length 66
2. 60 Degree Arc Deflectors 69
3. Summary 74

VI. CONCLUSIONS AND RECOMMENDATIONS 76

APPENDIX - GRAPHS OF PROCESSED DATA 79

LIST OF REFERENCES 83

INITIAL DISTRIBUTION LIST 86

LIST OF TABLES

TABLE I. Hot Wire Parameters 30

TABLE II. Empty Tunnel Velocity Data. 34

TABLE III. Tunnel Boundary Layer Above the Empty Step 35

TABLE IV. Deflector Porosity Details, Hole Diameter to Deflector Width Ratio 55

TABLE V. Circular Arc Deflectors 66

LIST OF FIGURES

Figure 1. AOR Class Ship 1

Figure 2. Generic Operating Envelope [Ref. 5] 7

Figure 3. Daytime Operating Envelope For BB-63 [Ref. 5] 8

Figure 4. Flow Over Flight Deck [Ref. 8:p. 7] 10

Figure 5. Mean Streamline Patterns About a Bluff Body [Ref. 10] 10

Figure 6. Separation Cavities For 2-D Flow [Ref. 12] 12

Figure 7. Centerline Streamline Patterns For Flow Reattaching To Top [Ref. 12] 12

Figure 8. Centerline Streamline Patterns For Flow Not Reattaching To Top [Ref. 12] 13

Figure 9. Wake of Hangar; DD-963 [Ref. 8:p. 27] 15

Figure 10. Backward Facing Step Flowfield [Ref. 15] 15

Figure 11. Reattachment-length Measurements Showing Dependence On The State Of The Separating Boundary Layer [Ref. 15] 17

Figure 12. Flow Structure Over 2-D Fence [Ref. 19] 19

Figure 13. Mean Streamlines At A Medium Dense And A Dense Windbreak [Ref. 22:p. 120] 21

Figure 14. The Wind speed Reduction Of Different Windbreaks (H= height of windbreak) [Ref. 22:p. 120] 22

Figure 15. NPS Low Speed Visualization Wind Tunnel [Ref. 8] 25

Figure 16. Schematic of Backward Facing Step 27
Figure 17. Deflector Mounts 28
Figure 18. Example of an F30/0%/0/12.5/30°, and a C60/57/0/30/30° Deflector 36
Figure 19. "PHOENICS" Generated Velocity Vector Field for the Open Step [Ref. 1:pp. 40] 41
Figure 20. Photograph of Flow Over an Open Step 41
Figure 21. "PHOENICS" Generated Velocity Vector Field for an F50/0%/0/50/0° Deflector [Ref. 1:pp. 54] 42
Figure 22. Photograph of an F50/0%/0/50/0° Deflector in the Wind Tunnel 42
Figure 23. "PHOENICS" Generated Velocity Vector Field for an F50/0%/0/30/30° Deflector [Ref. 1:pp. 58] 44
Figure 24. F50/0%/0/30/30° Deflector 44
Figure 25. "PHOENICS" Generated Velocity Vector Field for an F50/0%/0/12.5/0° [Ref. 1:pp. 50] 45
Figure 26. F50/0%/0/12.5/0° Deflector 45
Figure 27. F50/0%/0/30/30° Deflector 48
Figure 28. F38/0%/0/30/30° Deflector 48
Figure 29. F25/0%/0/38/30° Deflector 49
Figure 30. F25/0%/0/25/30° Deflector 50
Figure 31. F25/0%/0/50/30° Deflector 50

Figure 32. F25/0%/0/12.5/30° Deflector 51
Figure 33. F50/0%/0/30/45° Deflector 52
Figure 34. F38/0%/0/30/45° Deflector 52
Figure 35. F50/0%/0/12.5/45° Deflector 53
Figure 36. F38/42%/0/30/0° Deflector 55
Figure 37. F32/42%/0/30/0° Deflector 56
Figure 38. F38/46%/0/30/0° Deflector 56
Figure 39. F38/48%/0/30/0° Deflector 57
Figure 40. F38/56%/0/30/0° Deflector 57
Figure 41. F38/48%/0/12.5/0° Deflector 58
Figure 42. F25/51%/0/25/0° Deflector 59
Figure 43. F38/46%/0/30/30° Deflector 60
Figure 44. F38/48%/0/12.5/30° Deflector 60
Figure 45. F38/48%/0/25/30° Deflector 61
Figure 46. F38/48%/0/30/30° Deflector 61
Figure 47. F25/51%/0/38/30° Deflector 62
Figure 48. F25/51%/0/25/30° Deflector 62
Figure 49. F25/51%/0/12.5/30° Deflector 63
Figure 50. F38/48%/0/12.5/45° Deflector 64
Figure 51. F38/48%/0/0/-35° Deflector 65
Figure 52. F38/48%/0/0/-60° Deflector 65

Figure 53. C90/57/0/25/0° Deflector 67
Figure 54. C90/44/0/12.5/0° Deflector 67
Figure 55. C90/12/0/25/0° Deflector 68
Figure 56. C90/28/0/12.5/0° Deflector 69
Figure 57. C90/28/0/25/0° Deflector 69
Figure 58. C60/28/0/12.5/0° Deflector 70
Figure 59. C60/28/0/25/0° Deflector 71
Figure 60. C60/28/0/38/0° Deflector 71
Figure 61. C60/44/0/12.5/0° Deflector 72
Figure 62. C60/44/0/38/0° Deflector 72
Figure 63. C60/28/0/25/15° Deflector 73
Figure 64. C60/28/0/25/30° Deflector 74
Figure 65. C60/44/0/25/30° Deflector 75
Figure 66. C60/44/0/25/15° Deflector 75
Figure 67. Auto-correlation for the Step Centerline, 25 mm Elevation 79
Figure 68. Auto-correlation for the Step Centerline, 50 mm Elevation 80
Figure 69. Auto-correlation for the Step Centerline, 100 mm Elevation ... 80
Figure 70. Spectrum Function for the Step Centerline, 25 mm Elevation .. 81
Figure 71. Spectrum Function for the Step Centerline, 50 mm Elevation .. 81
Figure 72. Spectrum Function for the Step Centerline, 100 mm Elevation . 82

I. INTRODUCTION

The Navy's ability to conduct helicopter operations is more important today than ever before. Helicopters are a major contributor to the Antisubmarine and Antisurface Warfare mission areas and are equally important in the role of material supply between fleet ships, both underway and at anchor. The twin rotor helicopter, the H-46, is commonly used in this resupply mission because of its large load carrying ability and tolerance to varying wind conditions while hovering over ships.

The ability of the H-46 to operate in various weather and wind conditions is vital to the smooth and efficient operation of the fleet. However, an increasing number of "tunnel strike" mishaps, in which the rotor impacts the helicopter fuselage, have reduced the overall availability of the H-46. Most of these tunnel strike mishaps have occurred on AOR, LPA AND LPH type vessels, as seen in Figure 1, during rotor engagement or rotor shutdown, with winds of at least moderate strength.

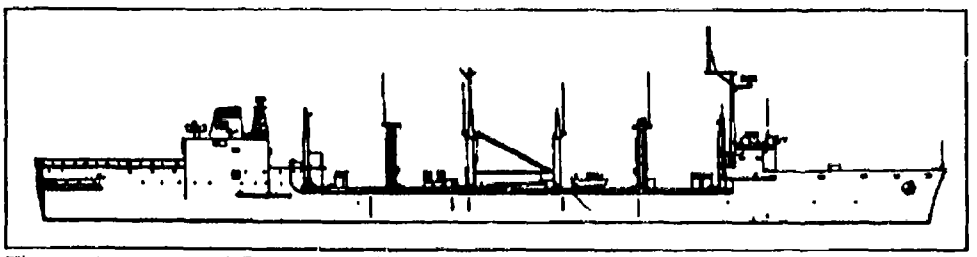

Figure 1. AOR Class Ship

It is generally thought that the main reason for most tunnel strike mishaps is the turbulent wind conditions encountered on the ship's helicopter deck. The only presently known solution to this problem is a reduction of the rotor engage/disengage envelope. The latter prescribes allowable safe operation limits based on the wind direction and speed.

The highly turbulent conditions often found on the helicopter deck are a result of the interaction between the wind, the ship's hull and superstructure. When Navy ships were first designed, their mission dependence on helicopters was not foreseen and so little attention was paid to the aerodynamics of the superstructure. Unfortunately, there has been little, if any, improvement in superstructure design, with regards to airflow, on today's newer ships. Thus, the environment around the ships, in which the helicopter must operate, remains quite hazardous.

The Naval Postgraduate School (NPS) has undertaken a series of studies on ship air wake tailoring, with the goal of reducing the level of turbulence and the size of the separated zones on the helicopter deck. This reduction will result in a larger engage/disengage envelope, which in turn, will increase the percentage of time that the H-46 and other helicopters can safely operate. This particular study is the second in the series at NPS to attempt to achieve this goal and will consider only the feasibility of such endeavors by tailoring a two-dimensional flow over a backward facing step. The first study, completed by Woolman [Ref. 1], was identical in purpose to the present study except that it was done numerically using the "PHOENICS" computational fluid

dynamics (CFD) code. This author collaborated with Woolman on the introduction and background portions of both studies. Consequently, the introductory chapters of Woolman's work [Ref. 1] and this study are essentially identical.

This analysis, in common with Woolman's [Ref. 1], was confined to two-dimensional flow. The tailoring of both three dimensional flow and flow over a forward facing step, which models the flow over the sides of the ship rather than over the superstructure, and are of paramount importance to the overall problem, are left to later studies. The general plan was to immerse a two-dimensional backward facing step in a simulated atmospheric boundary layer in the NPS low speed visualization wind tunnel and to attempt to modify the flow behind the step, through the use of strategically placed deflectors. An attempt was also made to verify Woolman's results [Ref. 1].

First, a more in-depth look at the role of the H-46 in fleet operations will be addressed; this will be followed by a short review of bluff body aerodynamics, ship air wakes, and any wake modification methods used up to the present. After the wind tunnel runs are completed, they will be analyzed, compared to each other and to Woolman's results. Results and recommendations will be made on step/deflector configurations for the next part of the program, which will be an attempt at the CFD tailoring of three-dimensional flows and their experimental verification.

II. BACKGROUND

A. HELICOPTER OPERATIONS

Navy fleets, which must travel worldwide, cannot hope to accomplish their mission without the "Mobile Logistic Support Force" (MLSF) ships. [Ref. 2:p. 1.1] This group of ships consists of the following ship classes: AE, AO, AOR, AFS, and AOE. These ships sail with the fleet carrying most of the supplies required for that particular deployment, such as food, fuel, and material goods. There are two basic methods to transfer these supplies from ship to ship: connected replenishment (CONREP) and vertical replenishment (VERTREP). [Ref. 3:p. 1.3]

CONREP is a method that involves two ships steaming side by side within 80 to 200 feet of each other and transferring supplies by means of cables strung between them. This method is commonly used for refueling ships and transferring loads which are too heavy for VERTREP.

The preferred method of replenishment is with helicopters, a method more commonly referred to as VERTREP. Supply items are placed in large cargo nets, lifted by the helicopters, and transferred to the appropriate ships. The specific advantages of VERTREP are:

1. Reduction in time required to replenish the supported forces or units.
2. Reduction or elimination of time that screening ships are off station.

3. Reduction of the number of personnel involved.

4. Capability of replenishing units in a dispersed formation.

5. Capability of replenishing units engaged in tasks which make it impossible for them to come alongside.

6. Capability of replenishing units in heavy weather conditions when alongside steaming is hazardous or impossible.

7. Capability of replenishing units on station in shallow water or at anchor.

As stated before, the twin rotor H-46 has become the helicopter of choice for this mission and its continuous availability in various weather and wind conditions has become vital in fleet operations. Tunnel strikes cause damage that must be repaired before the helicopter is available again and are numerous enough to threaten a reduction in the safe operating envelope of the H-46.

Though tunnel strikes typically occur at a very low rotor RPM, (usually at the start of rotor engagement or the end of rotor shutdown, when rotor RPM is about 20% of normal) they still pose a significant danger to the aircrew and ground personnel as well as to the aircraft. Through the middle of 1989, there have been over 100 such incidents aboard ships ranging from little or no damage to complete loss of the airframe. The dollar cost can range from just man hour costs when only inspections are required for a minor strike, to upwards of $500,000 for a tunnel strike which involves a sudden stoppage to the drivetrain system [Ref. 4:p. 4]. If the entire airframe is lost, the cost cannot be calculated because the H-46 is not in production and cannot be replaced.

Hidden costs are somewhat harder to measure, but are equally expensive. An interruption in the resupply operation can lead to changes in the entire fleet schedule. This may cause numerous other operations to be changed or canceled to allow the resupply mission to continue.

To avoid tunnel strikes while operating on shore, or from a ship, the helicopter crews use a chart which is essentially a go/no go chart which tells them if wind direction and speed will allow a safe rotor engagement or disengagement. The generic envelope for the H-46 is shown in Figure 2. There are also ship-specific envelopes, an example of which is shown in Figure 3.

These envelopes are developed through dynamic interface testing done by the Naval Air Test Center (NATC). It is a long, laborious and expensive process which is valid only for the particular combination of ship/ helicopter being tested. A description of the testing process is given by Madey and Whitmer [Ref. 6]. Unfortunately, due to the extraordinary variability of wind and sea state conditions, it is nearly impossible to document a completely safe operating envelope. This is certainly true for the H-46 and the AOR ship combination. A significant number of the tunnel strike incidents have occurred while operating inside of the rotor engage/disengage envelope.

This predicament has led to the suggestion that the problem may be solved by simulation [Ref. 7:p. 2]. To achieve this simulation accurately there is a need to predict the freestream airflow over the ship, the ship motion, and the motion of the helicopter. Healey [Ref. 7:pp. 14-58] looked at what has been done in these fields and lists over

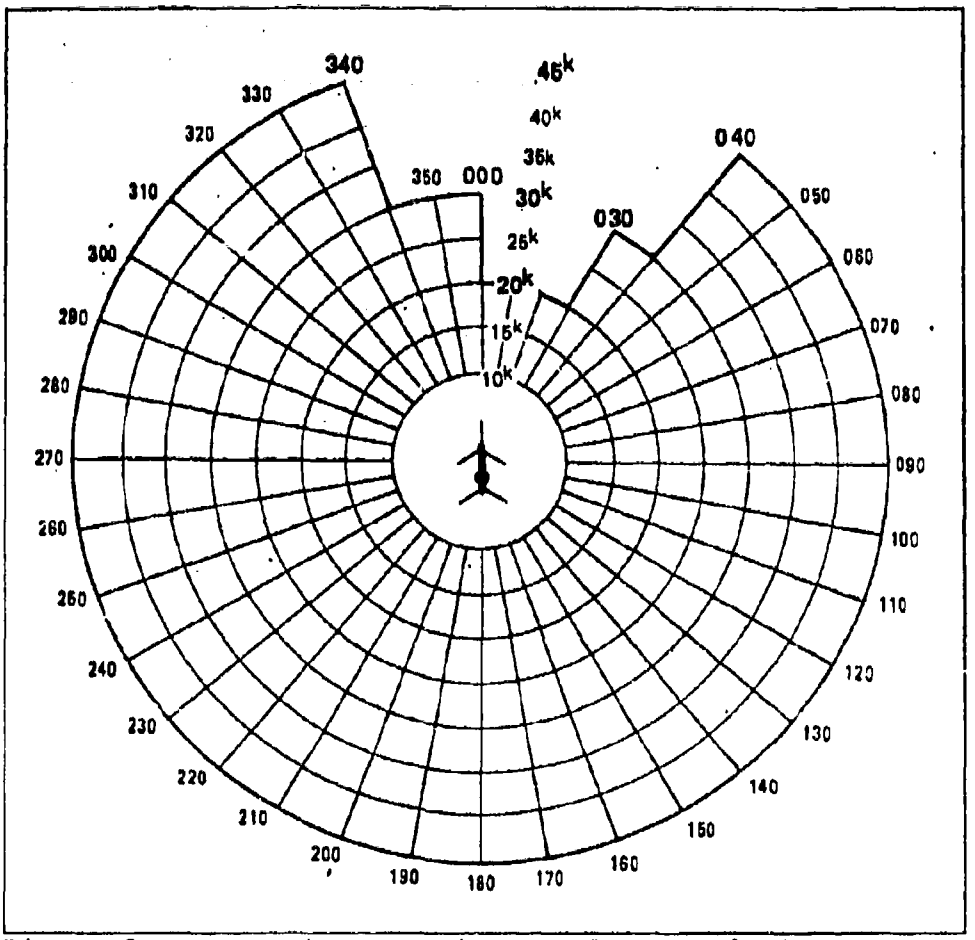

Figure 2. Generic Operating Envelope [Ref. 5]

100 references. The program underway at NPS is attempting to make detailed air-wake maps of model ships for scaling to full-size. So far, visualization of the flow around a model of a DD-963 class destroyer has been completed [Ref. 8] and a similar study of an AOR class ship is presently in progress [Ref. 9].

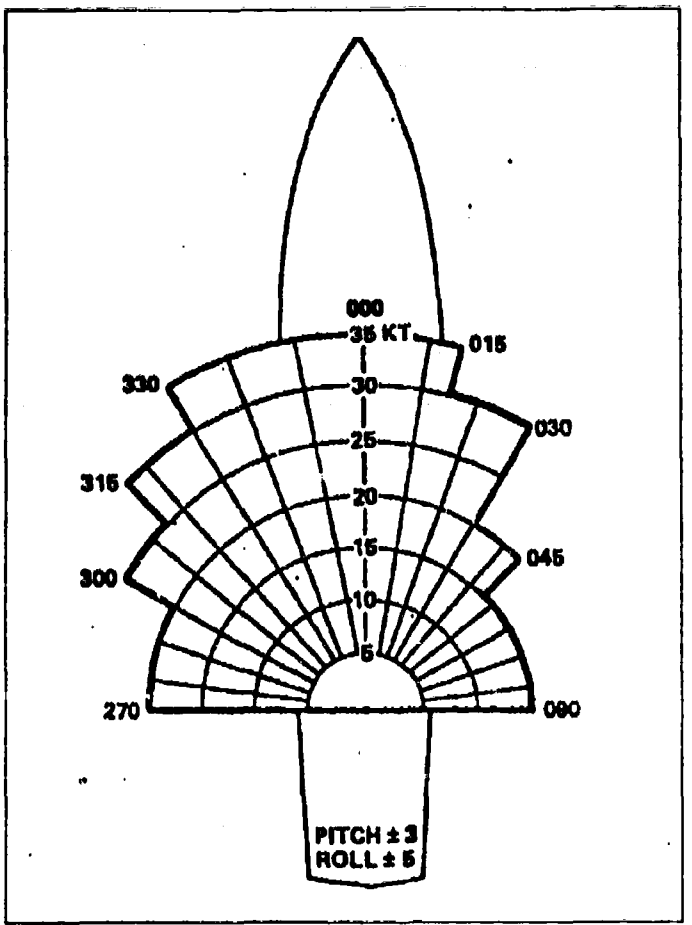

Figure 3. Daytime Operating Envelope For BB-63 [Ref. 5]

Until that time when a completely accurate rotor engage /disengage envelope is developed, other alternatives must be explored. This paper studies one such alternative; tailoring the ship airwake in order to reduce the size of the separation zones and the levels of turbulence encountered on the helicopter deck. This approach will not only eventually lead to a safer operating area for the helicopters but, if successful, will

increase the size of the rotor engage/disengage envelope, thus allowing the helicopters to operate a greater percentage of time.

B. BLUFF BODY AERODYNAMICS

Though the experimental part of this paper will be conducted as a two-dimensional problem, it is an important first step to understanding the three-dimensional airflow experienced by the ship, the helicopter deck, and subsequently the helicopter. Bluff body aerodynamics and their relationship to this problem will first be examined. This is not meant to be a detailed discourse on the subject, as the references to be cited more than adequately cover the subject.

By definition, a bluff body is one in which, for given flow conditions, there is a massive separated region in its wake. It becomes apparent, after first observing the design of any large class Navy ship, shown in Figure 1, and then a schematic of the observed flow over the flight deck of a model ship, shown in Figure 4, that Navy ships can indeed be considered three-dimensional bluff bodies.

To start to appreciate the complexity of the flow around a bluff body, one only has to look at a study by Hunt, Abell, Peterka, and Woo [Ref. 10:pp. 179-200]. They detected the presence of an inverted U-shaped vortex, whose ends remained in contact with the ground, on the downwind side of the body and numerous horseshoe vortices that wrap themselves around the upstream base of the body and trail downstream, as shown in Figure 5. In addition, turbulence causes the reattachment region to be highly unstable and alters the flow field around the body by producing increased mixing near the separated shear layers [Ref. 11].

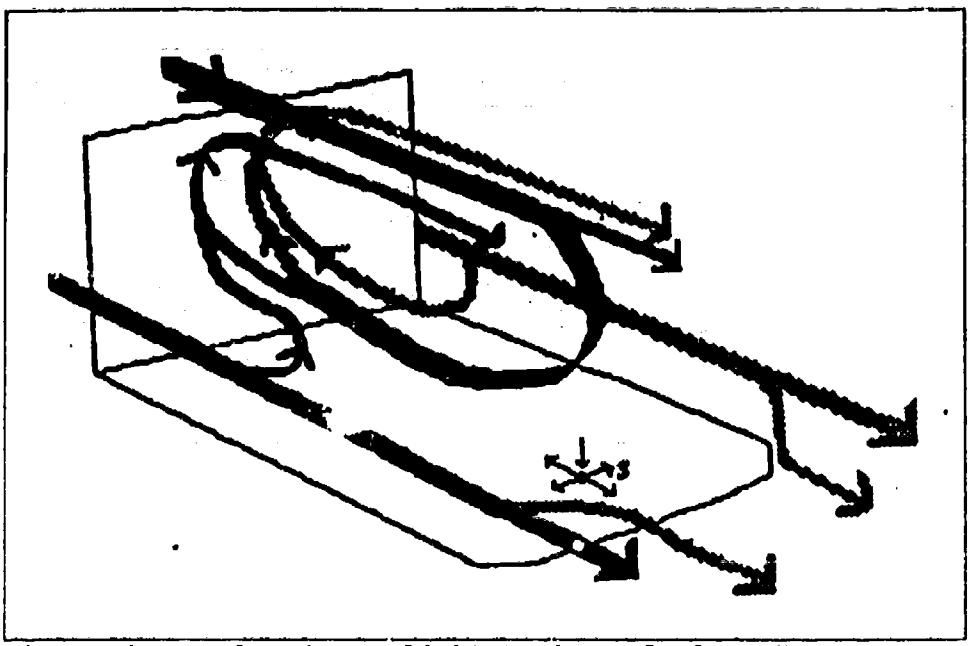

Figure 4. Flow Over Flight Deck [Ref. 8:p. 7]

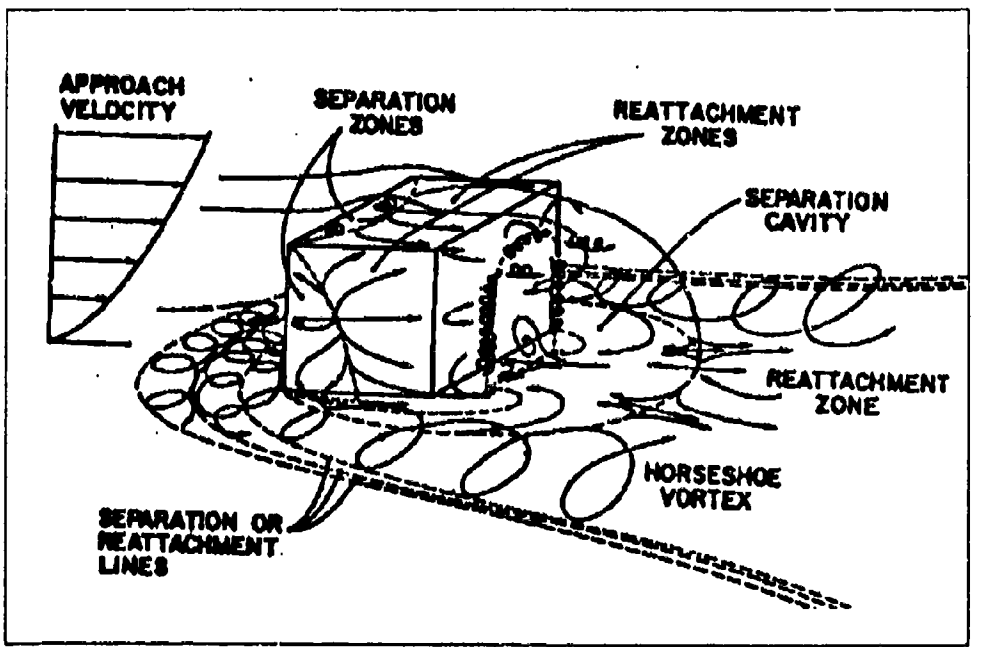

Figure 5. Mean Streamline Patterns About a Bluff Body [Ref. 10]

Trying to relate the flow around a simple bluff body to actual airflow over ships is an extremely difficult task. One can find only a few, and then poorly done, studies on the subject. As stated before, the present studies at NPS should rectify that situation soon. Until then, it is necessary to look elsewhere. One such area, where much time and effort have been expended, is in the area of wind flow around buildings and other obstacles [Ref. 12].

Recent investigations in the flow around buildings have advanced the understanding of physical flow processes occurring in the near and far wake region. But, according to Peterka et. al. [Ref. 12], even though there have been many studies in this area, there is still a high level of misunderstanding on how the winds actually flow around buildings. They believe that these misconceptions are probably caused by "conceptual extensions of two-dimensional flow". Figure 6 shows the separation zone for a two-dimensional object bounded by streamlines so that the cavities are closed. For a three-dimensional object, these separation lines are no longer valid. Studies which have been conducted in boundary layer wind tunnels [Ref. 12, 14] show that three-dimensional objects show fundamental differences in flow patterns relative to those of two-dimensional objects. Since this study is indeed based on two-dimensional flow relating to a three-dimensional problem, it is worthwhile to spend a little time looking at these differences.

As can be seen in Figures 7 and 8, the flow approaching the obstacle has separated at some distance upstream, at a point that is dependent, to the first order, on

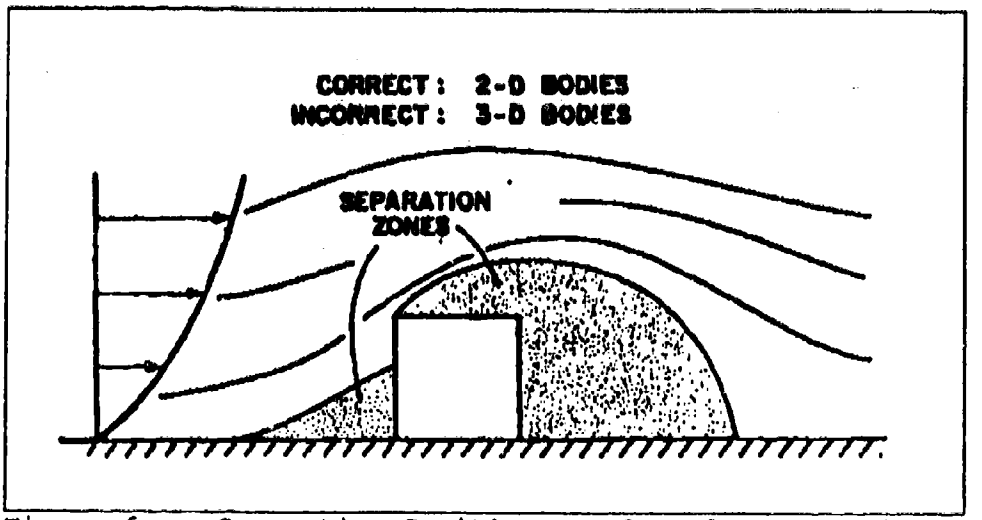

Figure 6. Separation Cavities For 2-D Flow [Ref. 12]

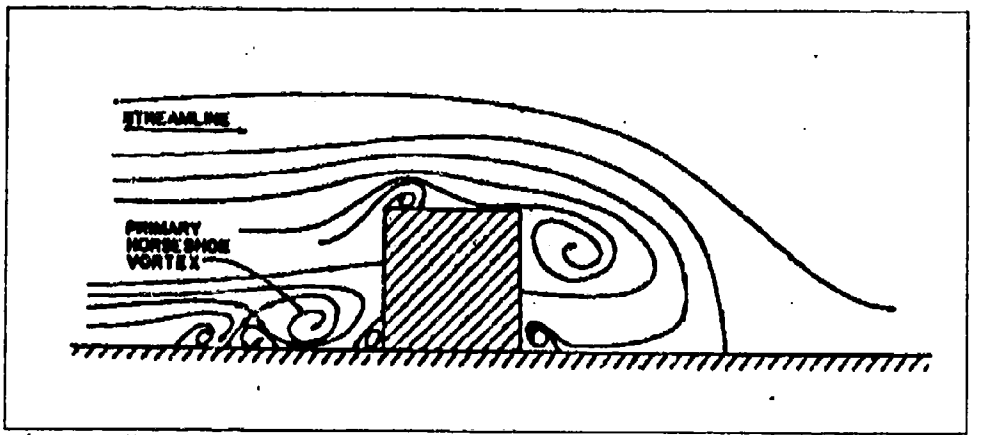

Figure 7. Centerline Streamline Patterns For Flow Reattaching To Top [Ref. 12]

building height-to-width ratio, building height-to-boundary-layer-height ratio and upstream surface roughness [Ref. 12]. The air in this separated flow strikes the building, flows downward and rolls up into a vortex. It then wraps around the building into the horseshoe shape that was discussed before. This horseshoe vortex can be

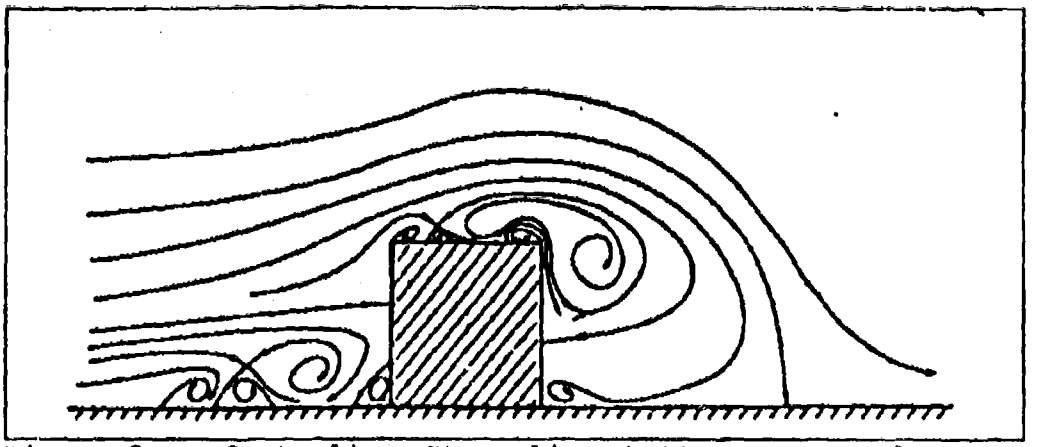

Figure 8. Centerline Streamline Patterns For Flow Not Reattaching To Top [Ref. 12]

identified in the flow for quite some distance downstream.

The wind that impinges on the front of the building forms a stagnation region somewhere near the top (about 2/3 the way up) depending on building height-to-width ratio. [Ref. 12] From this region, flow moves out toward all front edges of the object. Near these edges, it separates and may or may not reattach before reaching the back edge. This reattachment depends on many factors such as building-length-to-width ratio, height-to-length ratio and upstream roughness (which also determines the turbulence intensity in the approaching wind). Figures 5 and 7 show flow patterns for reattached flow and Figure 8 shows flow patterns for unreattached flow.

A separation cavity covers the rear face of the object. The cavity length is defined by the distance from the building to the centerline reattachment point downwind of the body, and is normalized by the building height. It can vary from two to six building heights [Ref. 10]. As a result of this variation, the reattachment "point" is

more accurately called a reattachment zone. This subject will be looked at more closely later.

Obtaining a clear picture of this separation cavity is quite difficult, due to the high level of turbulence inside this region. Figure 9, which graphically depicts the streak lines of helium bubbles, is a photograph of a helicopter deck from a flow-visualization study of a DD-963 class destroyer model. Bearing in mind that the size and shape of the cavity changes with ship yaw angle and, to some degree with pitching and rolling of the ship, it is little wonder that creating an accurate rotor engage/disengage envelope has been both difficult and unsuccessful.

C. FLOW OVER A BACKWARD FACING STEP

The next logical step is to proceed and review some important studies done on the flow over a backward facing step (BFS). Not only is this type of flow probably the easiest reattaching-flow scenario to observe, but it also comes very close to resembling the flow over the centerline of the helicopter deck at small yaw angles on the stern of most aviation ship configurations. Luckily, there have been several different type studies of this BFS. However, the present review will be confined to those dealing with turbulent two-dimensional freestream flow.

Although the backward facing step is the simplest of the reattaching flows, that fact is no way indicative of the complexity of the flowfield; it is still a very complex flow, as is illustrated by Figure 10. It can be observed that the upstream boundary layer separates at the sharp corner, forming a shear layer [Ref. 15]. This separated

Figure 9. Wake of Hangar; DD-963 [Ref. 8:p. 27]

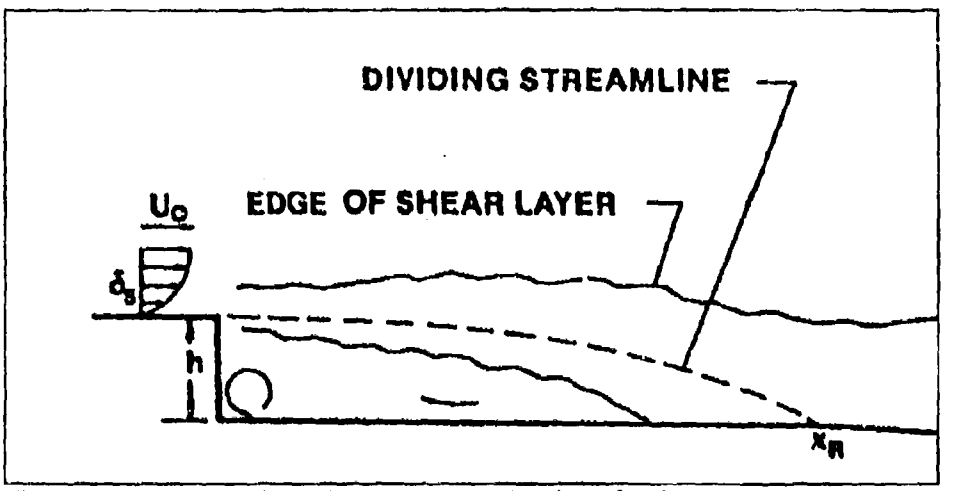

Figure 10. Backward Facing Step Flowfield [Ref. 15]

shear layer curves sharply downward in the reattachment zone. Then, after striking the floor, part of the flow is deflected upstream into the recirculating flow by a strong adverse pressure gradient. It would be incorrect to consider this recirculation area as a dead air zone. Backward flow has been measured at over 20% of the mean freestream velocity. [Ref. 15]

Eaton and Johnston [Ref. 15] have compared the results of several studies [Ref. 16-18] concerning the reattachment length, which together with the level of turbulence inside the recirculation area, are probably the most important parameters that characterize this flowfield. This work gives insight into the effect of varying the following four independent parameters: initial boundary-layer state, initial boundary-layer thickness, freestream turbulence and the aspect ratio.

It was found that the effect of changing the state (laminar/turbulent) of the separation boundary layer had a significant effect on the reattachment length. This relationship is illustrated in Figure 11. The flow apparently becomes independent of Reynolds number, based on momentum thickness, when the boundary layer is fully turbulent.

Data, in Eaton and Johnston's study, show that the reattachment length has a weak dependence on the effect of changing the state (laminar/turbulent) of the separation boundary layer. However, four other data sets with different values of the boundary layer thickness, but with similar other parameters, show the reattachment length having a much stronger dependence on the boundary layer thickness. The data suggests that further study is needed to resolve this issue.

The effect of freestream turbulence on the reattachment length has never been studied systematically. The few data sets that resulted from these studies, and documented in Eaton and Johnston's study, showed that fairly high levels of turbulence seemed to decrease the reattachment length. Again, further investigation is required.

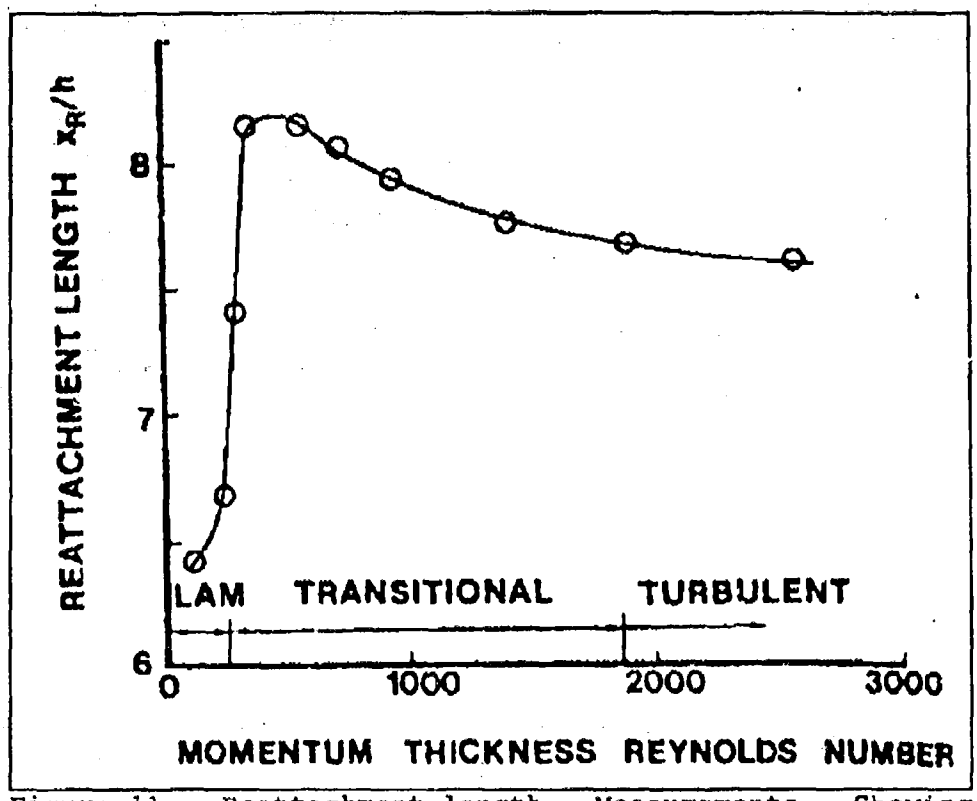

Figure 11. Reattachment-length Measurements Showing Dependence On The State Of The Separating Boundary Layer [Ref. 15]

The effect on the reattachment length, of the aspect ratio of the flow apparatus (channel height to step height), was also documented. These studies found that the effect was negligible for aspect ratios greater than ten. For aspect ratios less than ten, the reattachment length increases if the boundary layer at separation is laminar and decreases if it is turbulent.

The other important parameter, turbulence in the recirculation area, has also been measured for most of the data sets in Eaton and Johnston's survey. Though there seems to be a substantial variation in the peak values of turbulence and shear stress, the

turbulence-intensity measurements show a consistent pattern, when the maximum intensity is plotted as a function of streamwise distance. In almost all cases, the turbulence intensity reaches its greatest value approximately one step height upstream of reattachment and then decays rapidly in the downstream direction.

D. FLOW OVER A TWO-DIMENSIONAL OBSTACLE

Since a deflector will be used to direct the airflow over the backward facing step, it would be prudent to spend a brief time looking at the flow over a two-dimensional fence immersed in a turbulent layer on a flat surface. Such a study has been conducted recently by Atli [Ref. 19] who analyzed the flow field through the surface oil technique of flow visualization. He then obtained the longitudinal components of the mean velocities by using hot wire anemometry and applied corrections for flow reversal and turbulence.

Figure 12 shows the structure described by the flow visualization tests. Primary and secondary recirculation regions exist, both upstream and downstream of the fence, with both the downstream ones considerably larger. He observed that the relative height of the obstacle, in terms of the reference boundary layer and consequently the Reynolds number based on the height of the obstacle, is the parameter affecting the shape of the flowfield and the structure of the turbulence. Specifically the data indicated that the relative length of the primary recirculation region slightly increases when the relative height of the obstacle, and consequently the Reynolds number based

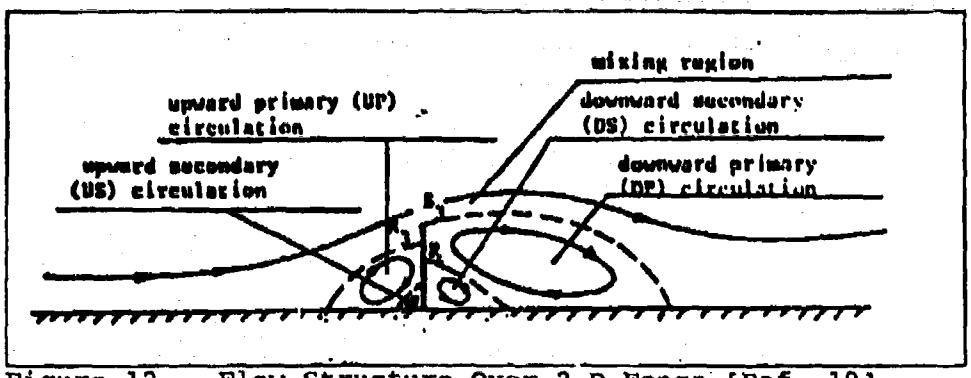

Figure 12. Flow Structure Over 2-D Fence [Ref. 19]

on obstacle height, increases. He did not observe this effect for the other recirculation areas; in fact, they remained the same size for the changes made.

Atli went on to compare his work with that of Sinha et al. [Ref. 20] who worked with flow over a backward facing step. He discovered that for 2-D flows with the same value of Reynolds number, the length of the primary recirculation region downstream of a fence on a flat surface is longer than that on the backward facing step. The reason for this is that the flow approaching the obstacle diverges from the horizontal before reaching the obstacle because of the upstream recirculation region. The flow approaching the backward facing step is horizontal and does not diverge.

Another conclusion which Atli reaches, which has some relevance to the present study, is that the reverse velocity profile in the recirculation region increases with height of the step and therefore with the height based Reynolds number. This increase in obstacle height and Reynolds number also increases the maximum turbulence intensity in the mixing region.

E. FLOW MODIFICATION

Though no studies can be found that attempt to modify the airflow over a backward facing step through the use of deflectors, one study by Kato et el. [Ref. 21] did attempt to control the wake behind a bluff-based body and to reduce its form drag through the use of circular-arc guide vanes. However, the paper was written in Japanese, and as of this writing an English translation has not been located. Several studies published in English, of the airflow over and through fences and shelterbelts were located. These studies generally deal with modifying the airflow, so as to protect crops or provide comfort for humans, through the use of various type windbreaks. Much of this information is applicable to our current study and will be used in the modelling portion of the problem.

Windbreaks and shelterbelts have played, and continue to play, an important part in protecting man and his environment. It was with this in mind that the World Meteorological Organization, at its second session in 1958, first set up a working group on windbreaks. They worked out a plan for long-term experiments to assist in regional planning of windbreaks and shelterbelts for research purposes. The results of their work were published in 1964 [Ref. 22] and much of what they concluded is still valid today.

One of the general conclusions of their study, shown in Figure 13, was that beneath the peak airflow over a windbreak is the zone of greatest wind reduction. At that time it was called a "dead calm area" by Kreutz. [Ref. 22: p. 72] This term is

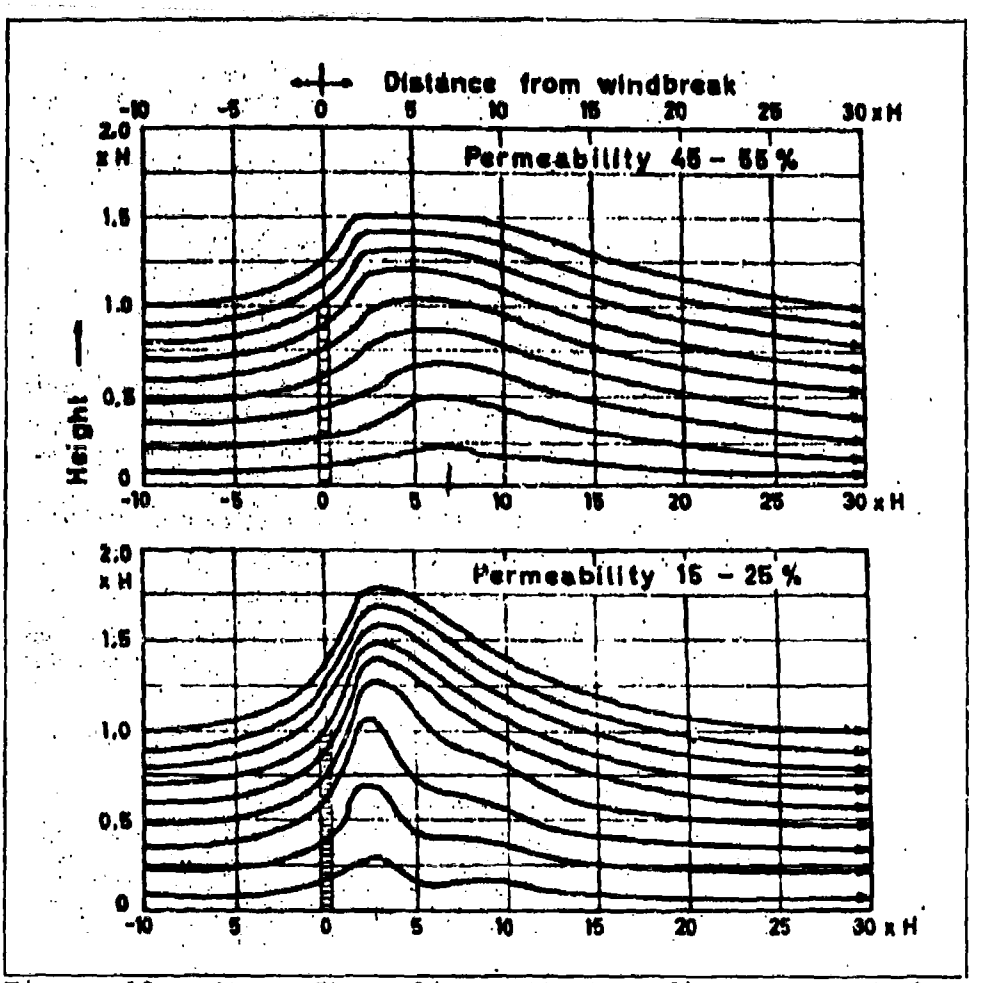

Figure 13. Mean Streamlines At A Medium Dense And A Dense Windbreak [Ref. 22:p. 120]

really a misnomer, as has since been shown [Ref. 19]. Figure 14 illustrates the reduction in horizontal wind behind a windbreak as a function of windbreak permeability. This figure also shows that the lower the porosity of the obstacle, the nearer to the obstacle the "calm" area is located.

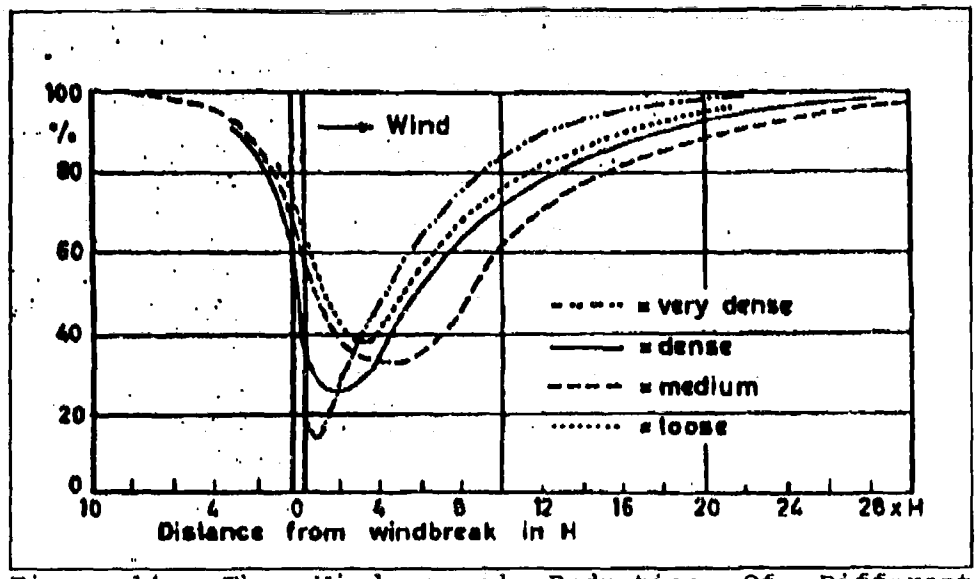

Figure 14. The Wind speed Reduction Of Different Windbreaks (H= height of windbreak) [Ref. 22:p. 120]

The crucial parameter for wind reduction behind shelterbelts was, therefore, determined to be the shelterbelt's density, or porosity. The less porous, the more wind reduction, but for only a very small area immediately behind the shelterbelt. Then, as the porosity increases, the horizontal wind velocity increases slightly, but the area of protection, measured downwind, also increases. The overall best protection, which extended six to seven shelterbelt heights downstream, was thought to require about 50% porosity.

In 1981 Perera [Ref. 23] showed that the normalized mean wind velocity through a porous fence was independent of the form of the fence construction. Small holes, large holes, and even horizontal slat fences seemed to have no significant effect on altering the results for a given porosity. Several other studies have also confirmed

Perera's results. Another of his conclusions was that, as the porosity increased, the recirculation bubble decreased in size and moved downstream. His results showed that the recirculation bubble existed only for fences with porosities less than 30%.

In summary, wake velocities behind wind breaks and shelterbelts increase but the turbulence intensity decreases with increasing porosity. This same principle is expected to be true for any deflector that might be mounted on a backward facing step.

III. EXPERIMENTAL APPARATUS

A. WIND TUNNEL

This study was conducted in the NPS low speed flow visualization wind tunnel, which was already modified to simulate the atmospheric boundary layer. While not tailored specifically for this study, it did provide a thick turbulent boundary layer approaching the backward facing step.

The tunnel, illustrated in Figure 15, is an open circuit design consisting of a 9:1 square bell contraction cone inlet followed by a square test section and a variable pitch fan. The inlet to the contraction cone is a 4.5 X 4.5 meter (15 X 15 foot) square that contracts to the 1.5 X 1.5 meter (5 X 5 foot) test section. The air enters through a three inch honeycomb, passes through the contraction cone and down the 7 meter (22 feet) long test section before exhausting to the atmosphere.

An observation room is located next to the test section and houses all the necessary equipment. The inner test section wall on the observation side is almost completely glass, which allows easy viewing and photography. Lighting of the flowfield can be accomplished through glass windows both in the top and far side of the test section, or from well downstream in the tunnel. All opaque surfaces are painted flat black to minimize reflectivity.

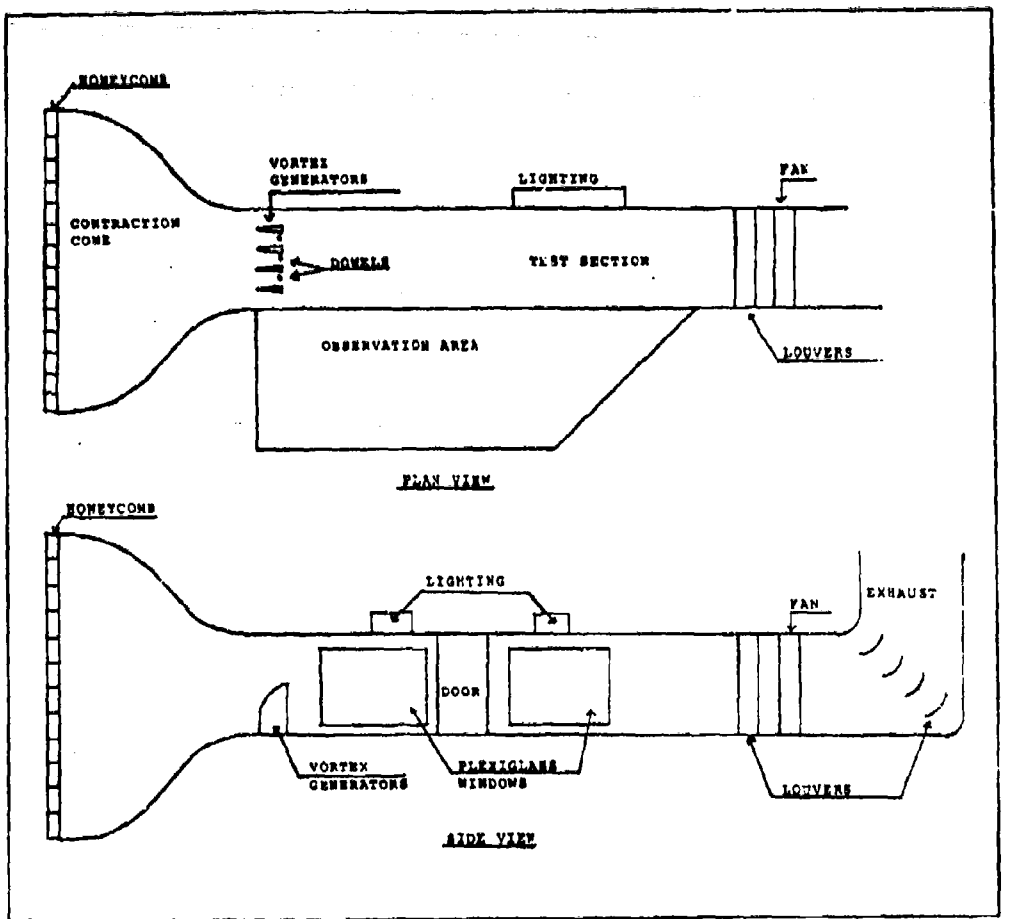

Figure 15. NPS Low Speed Visualization Wind Tunnel [Ref. 8]

The method used to produce the boundary layer was a modification of the method described by Counihan. [Ref. 25] It consisted of four vortex generators and four conical dowels that generate the shear and turbulence. The vortex generators were constructed of aluminum and styrofoam cut in a quarter elliptical shape when viewed from the side. They were 742 millimeters high, 381 millimeters long in the flow direction at the base and tapered in the flow direction from about 6 millimeters at the

top to 72 millimeters thick at the base. Conical dowels were placed between the vortex generators to produce a more uniform boundary layer. They were also 742 millimeters high and tapered from 6 millimeters on top to 76 millimeters diameter on the bottom. Additional small dowels were taped to the sides of some of the vortex generators to achieve a more uniform flow across the test section than was possible with the vortex generators and the large conical dowels alone.

These modifications resulted in a 742 millimeter thick boundary layer which is more than adequate for the present study. The Reynolds number based on the step height and the freestream velocity at the top of the boundary layer was 26800. The ratio of boundary layer thickness to step height was 5.8, which was almost twice the ratio of any literature cited.

B. THE STEP

The two dimensional backward facing step, 127 millimeters high by 457 millimeters, pictured in Figure 16, was constructed of 12 millimeter plywood and painted black. A 508 millimeter ramp was used, on the upwind side that leads to the step top, to ensure the boundary layer at the step was fully developed but was not influenced by the leading edge of the step. To achieve two dimensional flow, side walls were added that extended 304 millimeters windward of the ramp to 914 millimeters downwind of the step. These walls were made of plywood except for one half of the wall on the observation side, which was made of acrylic to allow viewing and photography.

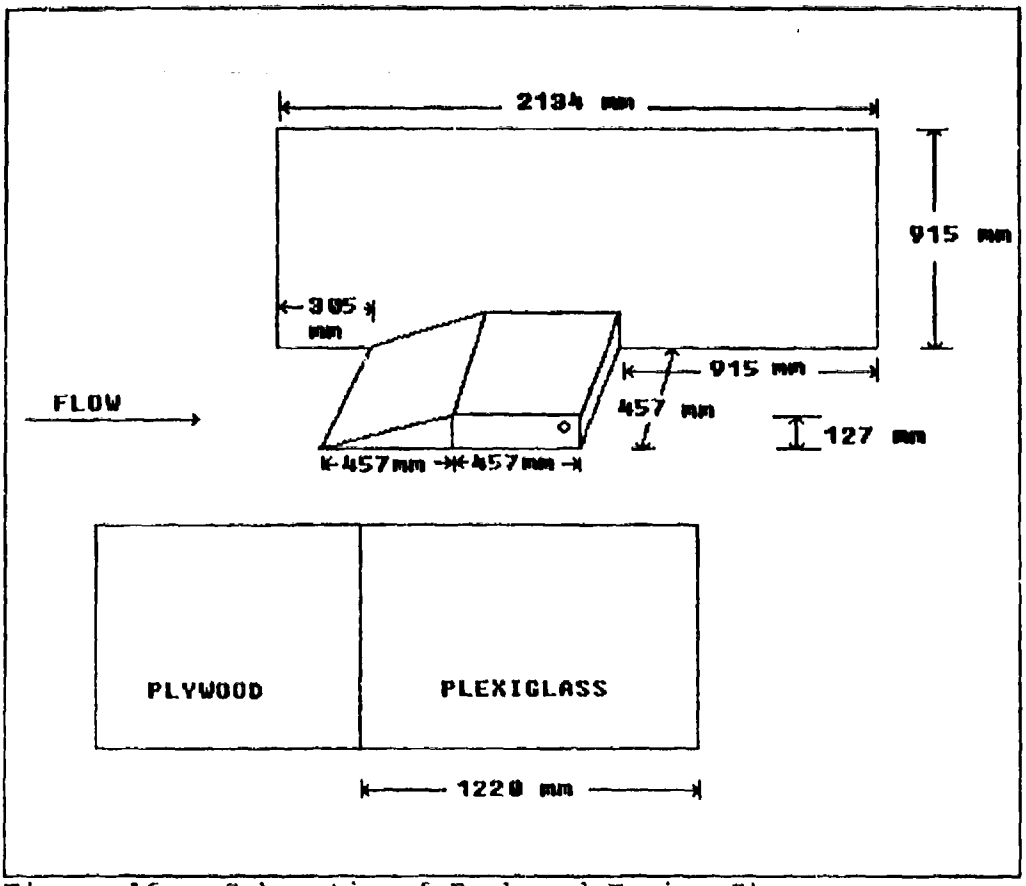

Figure 16. Schematic of Backward Facing Step

The mounting apparatus for the deflectors diagramed in Figure 17, consisted of two three-eighth inch bolts (called mounting bolts) extending through the step 250 millimeters apart. These bolts were mounted in threaded holes in a larger bolt (called the base bolt) that extended the width of the step. This allowed the angle of the deflectors to be adjusted both by turning the base bolt and the deflector itself. The distance from the deflector to the step was adjustable by turning the mounting bolts

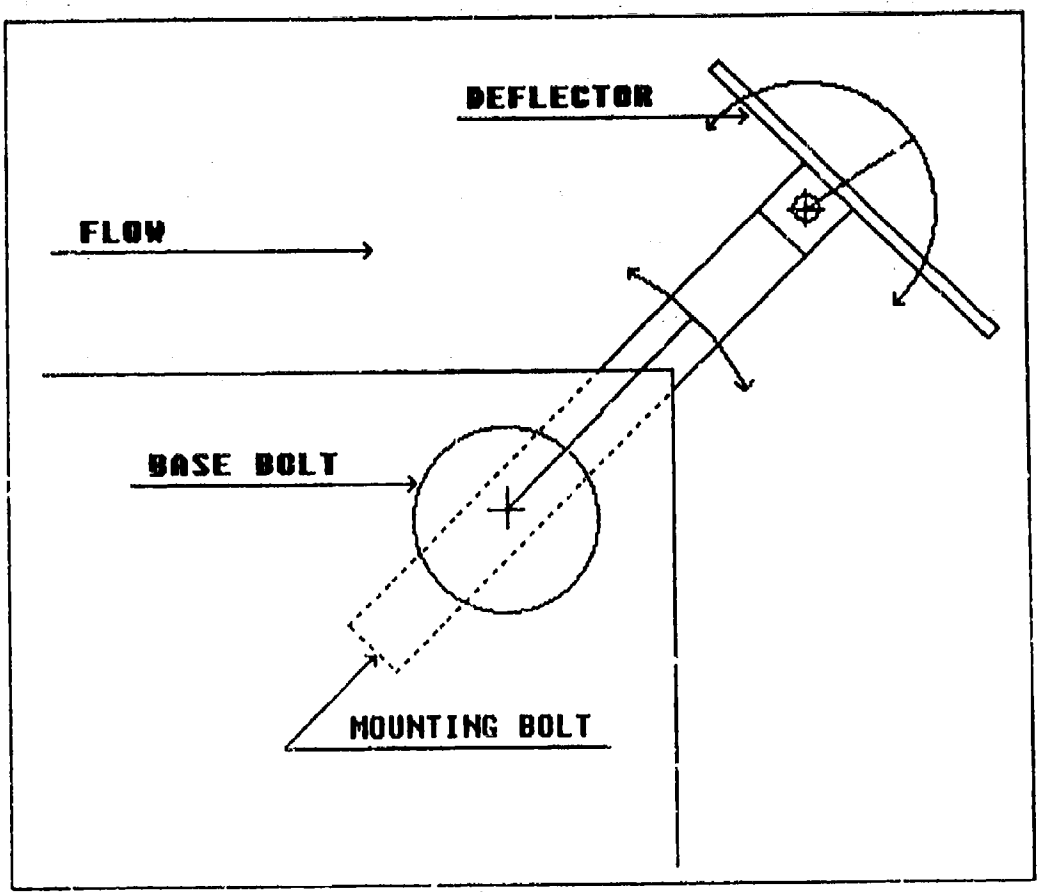

Figure 17. Deflector Mounts

into, or out of, the base bolt, which had tapped holes, thereby adjusting their length. Slots were cut in the step to accommodate the mounting bolts.

C. THE DEFLECTORS

The deflectors spanned the step and were constructed of one sixteenth inch thick aluminum or steel. Flat deflectors were either 25, 38 or 50 millimeters wide. Each deflector was either nonporous or had porosities varying from about 42 to 56 percent. The circular arc deflectors, which were all nonporous because of insufficient time to

consider porous types, were either 60 or 90 degree arcs. The radii of curvature available were: 57, 44, 28, and 12 millimeters. Both the leading and trailing edges of the circular arc deflectors were beveled to provide a sharp edge.

D. HOT WIRE ANEMOMETER

A Dantec 55R91 3-D hot wire probe was used in this study. Table I lists its parameters. [Ref. 26:p.9] The probe consisted of three mutually perpendicular sensors mounted such that the horizontal direction of the flow is inside a cone of 70.4 degrees (35.2 degrees in any direction from the axis). This configuration is preferred to avoid support prong interference and thermal crosstalk between the sensor films due to their hot wakes. [Ref. 27:p. 23]

E. THE CONSTANT TEMPERATURE ANEMOMETER UNIT AND BRIDGE

The Dantec 56C01 Constant Temperature Anemometer (CTA) and the 56C17 Bridge form a complete constant temperature anemometer, producing an analog output signal proportional to the velocity of the fluid flow over the probe. The leads of the triple wire probe are each connected to a bridge using a 20 meter coaxial cable to form one arm of a Wheatstone bridge. The CTA provides the capability for the operator to balance the bridge resistance with the probe's, leads' and cables' resistances by adjusting internal resistances and to select the overheat ratio defined by, $a=(R-R_o)/R_o$, where R_o is the ambient temperature resistance and R is the heated sensor resistance [Ref. 28:p. 8]. The CTA also has an amplifier which attempts to maintain the circuitry in balance during operation.

TABLE I. Hot Wire Parameters

	TRIPLE WIRE
Material	**Tungsten**
Diameter	8.89 microns dia.
Active length	1.25 mm
Ambient (20 C) Temperature resistance	3.5 ohms wire one 3.5 ohms wire two 3.5 ohms wire three
Temp. Coef. of Resistance	0.42% per degree C
Max. Temperature	300 C
Min. Velocity	0.2 m/s
Frequency Limit F_{cmax}	300 Khz

F. THE ANALOG TO DIGITAL CONVERTER

The output of the CTA was converted to a digital signal using the Metrabyte Corporation 12 bit model DASH-16 successive approximation converter. It has a maximum throughput rate of 60 kHz, software controllable and a voltage range of +/-10 volts. It also has a low-drift, fast settling sample and hold amplifier that ensures the signals from all three probe channels are read virtually simultaneously. [Ref. 29:p. 1-3]

G. THE COMPUTER

A Compaq 386/25 micro computer, HP 7475A Graphics Plotter and an HP Laserjet IIP printer were utilized during this study. The Compaq 386/25 runs at 25

Mhz with an Intel 80386 central processing unit. It was used to acquire all data using Metrabyte Streamer software and to process it using Dantec software.

H. ACQUISITION AND PROCESSING SOFTWARE

The Metrabyte Streamer software was used for all data acquisition. This software package is a high speed hard disk data transfer utility. It provides for continuous analog to digital (A/D) data transfer to hard disk.

The Dantec "acqWIRE" software was used to read the Streamer created files and to perform all calibration, statistical analysis, spectrum/correlation and flow-field plots of the result. All subroutines are menu driven and contain options for probe calibration, calibration data and error plotting, data acquisition, conversion to reference coordinate system and data storage.

Data analysis options include computation of the mean velocity, root mean square velocity (RMS), turbulence intensities, skewness, flatness, cross moments and turbulence kinetic energy. It will also compute and display windowed and/or block averaged power spectral densities and auto- or cross-correlations.

I. HELIUM BUBBLE GENERATION

The helium bubble generator used was built by Sage Action Inc. and required compressed air, helium and bubble film solution sources. These components were metered to a bubble generating nozzle located on a bubble filter which acts as a centrifuge. The heavier-than-air bubbles spin out, hit the sides of the cylinder and

break. The lighter-than-air bubbles spiral inward and hit the center tube or the top and also break. The neutrally buoyant bubbles continue circulating and are collected using a tube which extends from the top to the lower center of the filter. These bubbles are then forced through a flexible tube and led in the flow, ahead of the step in an unobtrusive manner.

J. LIGHTING

Illumination of the flowfield turned out to be much easier than expected. A single arc lamp, located on the tunnel floor, on centerline about 1.6 meters downstream was directed at the center of the back of the step. It was positioned to illuminate as little of the floor as possible, while still lighting the back and top of the step. This arrangement illuminated the bubbles that flowed down the centerline, making them visible, while any bubbles that might have strayed well off centerline were not.

K. STILL PHOTOGRAPHY

All still photographs were taken with a Hasselblad 2000 FCW medium format camera utilizing a Tessar 110 mm f2 lens and Kodak TMAX ASA 400 film. Other accessories included a Bogen tripod, various filters, backs, and a time extender.

L. VIDEO

Video equipment used were a Panasonic WV-1850, 800 line closed circuit camera with a 25 mm f1.4 automatic iris lens, a Panasonic WV-5470, 850 line monitor and a Mitsubishi HS-423UR, 440 line super-VHS cassette recorder.

IV. EXPERIMENTAL PROCEDURE

A. TUNNEL CALIBRATION

This study began with the calibration of the tunnel flow. Using the hot wire anemometer, the flow characteristics were mapped as a function of both transverse and vertical positions. The vortex generators and conical dowels were slightly modified by taping smaller cylindrical dowels to the sides of the conical dowels until an acceptable simulation of the atmospheric boundary layer over a rough sea was produced. Table II shows the results for the center area of the wind tunnel, which was the area of interest; the velocities are in meters per second, the Y distances are in millimeters, U_o is the mean velocity taken at the top of the tunnel, well out of the boundary layer, and σ is the standard deviation of the velocities at each height.

The velocity and turbulence intensity boundary layer information taken above the open step is presented in Table III. The measurements were taken 3 millimeters upstream of the step edge and at the indicated height above the step. Graphs of the spectral function and the auto-correlation functions for the 25, 50 and 100 millimeter heights can be found in the Appendix. Due to both hardware and software problems with the hot wire anemometry system, time did not allow a more detailed analysis.

A least squares curve fit to the velocity data of Table III yields a value of 0.09 for n in the equation; $\frac{u}{u_{600}} = (\frac{Z}{Z_{600}})^n$. This compares with the value of n=0.11 for

TABLE II. Empty Tunnel Velocity Data.

Y Dist. from far wall in NPS Smoke Tunnel U_o = 2.83 m/sec	Z - Height from floor in millimeters								
		50	75	100	150	200	250	350	500
	450	1.63	1.78	1.87	1.91	1.96	1.98	2.10	2.22
	600	1.66	1.75	1.83	1.86	1.97	1.97	2.10	2.15
	750	1.67	1.78	1.88	1.95	2.02	2.03	2.11	2.13
	900	1.65	1.82	1.89	1.96	2.07	2.09	2.15	2.23
	1050	1.67	1.78	1.89	1.97	2.05	2.05	2.14	2.23
	U_{ave}	1.66	1.78	1.87	1.93	2.01	2.02	2.12	2.19
	U_{ave}/U_o	0.59	0.63	0.66	0.68	0.71	0.71	0.75	0.77
	σ	.017	.025	.025	.045	.048	.050	.023	.048

the empty tunnel. It is noted that the ramp/step combination produces a minor overshoot in the velocity profile.

The turbulence intensities are within an acceptable range of values [Ref. 7 and 32] for simulation of the atmosphere over a rough sea. The length scales, estimated by Taylor's frozen turbulence hypothesis from Figures 67-69 in the Appendix, are 31, 50 and 28 millimeters respectively, for the 25, 50 and 100 millimeter levels. These values compare with the open tunnel values of 34, and 27 millimeters at 50 and 100 millimeter levels. It is apparent that the eddies become stretched as they travelled up the ramp.

The spectra, given by Figures 70-72 in the appendix, show peaks near 1-3 Hertz, followed by two distinct and separate negative slopes, as the frequency increases. The first is the rather faint, but distinct presence of the inertial sublayer This faintness

TABLE III. Tunnel Boundary Layer Above the Empty Step

Height Above Step in mm	Mean Velocity in m/s	U/U_{600}	Turbulence Intensity
7	2.36	.77	11.4
12	2.54	.84	10.1
17	2.64	.87	9.6
25	2.78	.91	8.0
37	2.89	.95	6.1
50	2.92	.96	6.3
75	3.03	1.00	5.7
100	3.13	1.03	4.7
200	3.30	1.08	3.3
350	3.45	1.13	3.1
500	3.07	1.01	2.8
600	3.04	1.00	2.3

appears to be a consequence of the sampling rate and filter setting. The spectra are very similar to those of the open tunnel. A more complete discussion of these matters appears in Reference 32.

B. FLOW VISUALIZATION

1. Deflector Placement

The deflectors, and the positions used, are referred to by the width, the porosity, the placement of the lower or downstream edge which later will be referred to as the offset, and the angle the deflector makes with the vertical. A flat, 50

millimeter, 40% porous, deflector placed with the trailing edge 0 millimeters above and 30 millimeters downstream of the step corner at a 30 degree angle to the vertical, will be referred to as an F50/40%/0/30/30° deflector. In referring to a circular arc deflector, the width is replaced by the arc size in degrees, the porosity is replaced by the radius of curvature since only non-porous arcs were used and the trailing edge angle is the angle the tangent of the arc of the trailing edge subtends with the vertical. A curved, 60 degree arc, 57 millimeter radius of curvature deflector placed with the trailing edge 0 millimeters above and 12.5 millimeters behind the step corner at 30° will be referred to as a C60°/57/0/12.5/30°. Examples of each type deflector can be seen in Figure 18.

The deflectors were initially placed in the positions that showed promising results when computed analytically by Woolman [Ref. 1]. However, Woolman did not run as wide a variety of deflectors as were available in this study and he ran no curved deflectors, so there is no particular guidance as to placement for most of the deflectors used.

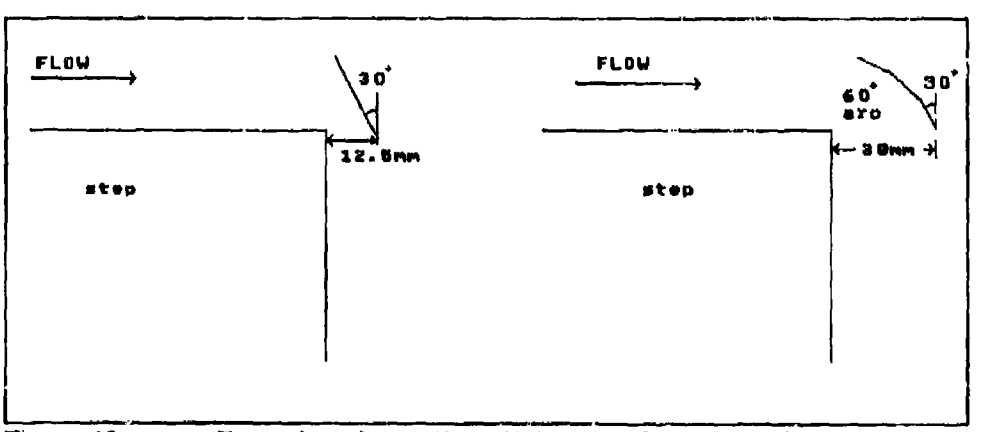

Figure 18. Example of an F30/0%/0/12.5/30°, and a C60/57/0/30/30° Deflector

2. Helium Bubbles

Initially, qualitative results were obtained at each deflector position using helium bubbles. This was the easiest flow visualization method available, so a large number of deflectors and positions could be viewed quickly and a general insight to the flow pattern gained. Bubbles were injected parallel to the flow on the centerline of the step approximately in the center of the ramp. This position was close enough to the back of the step to prevent them from spreading out very much before reaching the back of the step, but far enough away to allow the small disturbance of the injection to settle out before the back of the step was reached. Both long exposure still photos and video photos were taken and analyzed.

C. HOT WIRE ANEMOMETRY

It was desirable to take hot wire measurements inside the recirculation region but, at the very high turbulence levels that exist there, the available probe was useless. Since a pulsed wire anemometer was not available, measurements were planned only outside the recirculation region for the most promising deflector positions. The measurements both above the deflectors and above the shear layer behind the step were also not taken for the reason stated in Section IV.A.

While hot wire anemometry did not allow gathering quantitative data in the recirculation region, the combination of helium bubbles and video did allow a rough estimate of velocities. The video tapes were analyzed one frame at a time and measurements taken on the screen of bubble movement from frame to frame. Since the

camera speed is known it was a simple matter to roughly estimate the flow speeds. The estimates were made by putting an object of known length in the tunnel and measuring it on the video monitor. A conversion factor was thus calculated. The actual measurement of the bubble displacements was also complicated by the fact that the flow was strictly not two dimensional. The bubbles did move horizontally perpendicular to the general flow direction. To compensate for this, the velocity of the fastest bubble in any region was taken as the velocity of that region.

V. RESULTS AND DISCUSSION

A region of special interest to this study is the region of space that would be occupied by the main rotor blades of the helicopters during start-up and shut-down. Hereafter this region will be referred to as "the region of interest". It ranges from one half, to two full step heights downstream of the step and one fourth, to three fourths of a step height off the floor. In the discussion that follows, unless otherwise indicated, comparisons of the properties of a given flow and the reference BFS flow refer to this particular area.

It should be noted, before viewing the figures, that a great deal of detail was available in the original photographs and was lost in the half-tone production process. The combination of the original photographs and the video, allowed much more detailed study of the flow than is apparent from the figures.

A. VALIDATION OF "PHOENICS" CFD RESULTS

Before a comparison to the "PHOENICS" results can be made, a short discussion of the program and previously-noted weaknesses, is in order. The two equation k- ε turbulence model was used by Woolman [Ref. 1]. This model is widely used and gave reasonable results for the velocity field around a cube in a study by Muakami and Mochida [Ref. 30]. However, a study by Yeung and Kot [Ref. 31] revealed that the

reattachment lengths obtained were underpredicted when compared to studies. In other words, the flow field pattern did not extend as far downstream as has been observed.

This was true for all the cases compared in the present study. In one case the underprediction was extreme, resulting in very poor agreement with the experimental results. Figure 19 shows the vector velocity field for the open step as predicted by "PHOENICS" and Figure 20 is a photograph of the helium bubble streaklines over the open step in the wind tunnel. A comparison reveals the underpredicted reattachment zone calculated by "PHOENICS" but otherwise good agreement in the general shape of the flow pattern. "PHOENICS" predicts the reattachment zone to be at about 3 to 4 step heights (H) and the center of the recirculation zone to be at about 1.3 H while the photo reveals the actual reattachment zone to be at about 5 H and the center of the recirculation zone to be at about 2 to 3 H. Analysis of the video reveals that the ratios of the velocities in the recirculation zone to those above the step are roughly the same for both "PHOENICS" and the experimental results. This is in agreement with the ratios cited the literature. The reattachment length was also in agreement with previous studies. Eaton and Johnston's [Ref. 15] review of studies revealed several with reattachment lengths in the 5 to 6 H range.

The underprediction of the downstream flow pattern remained true for all the deflector positions compared. Figure 21 and 22 show the results using an F50/0%/0/50/0° deflector. The "PHOENICS" flow pattern is generally correct, showing the basic S shaped flow immediately downstream of the deflector. However, the small

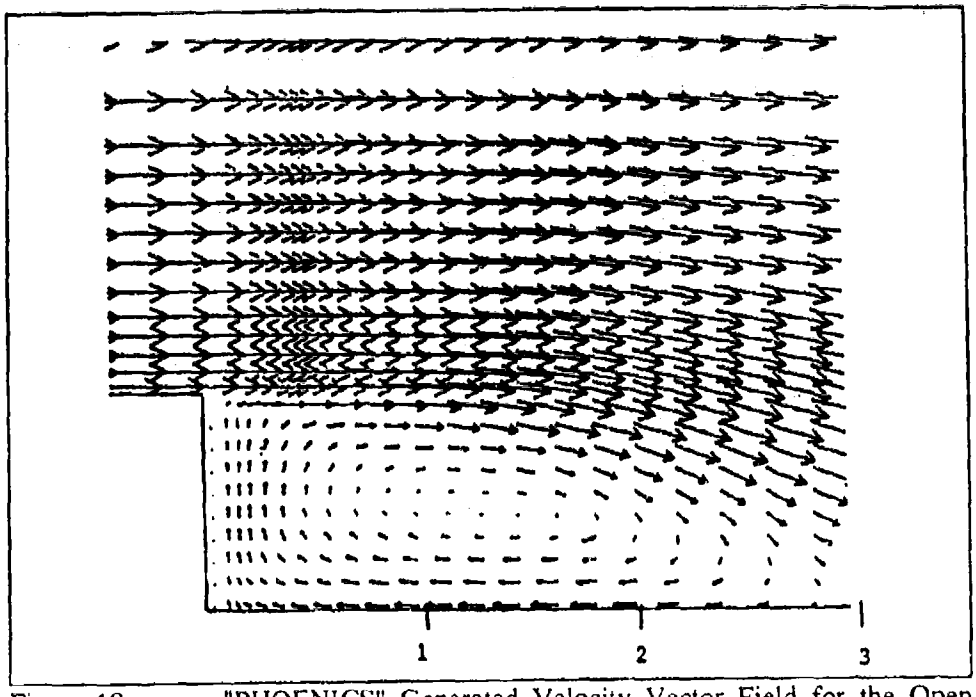

Figure 19. "PHOENICS" Generated Velocity Vector Field for the Open Step [Ref. 1:pp. 40]

Figure 20. Photograph of Flow Over an Open Step

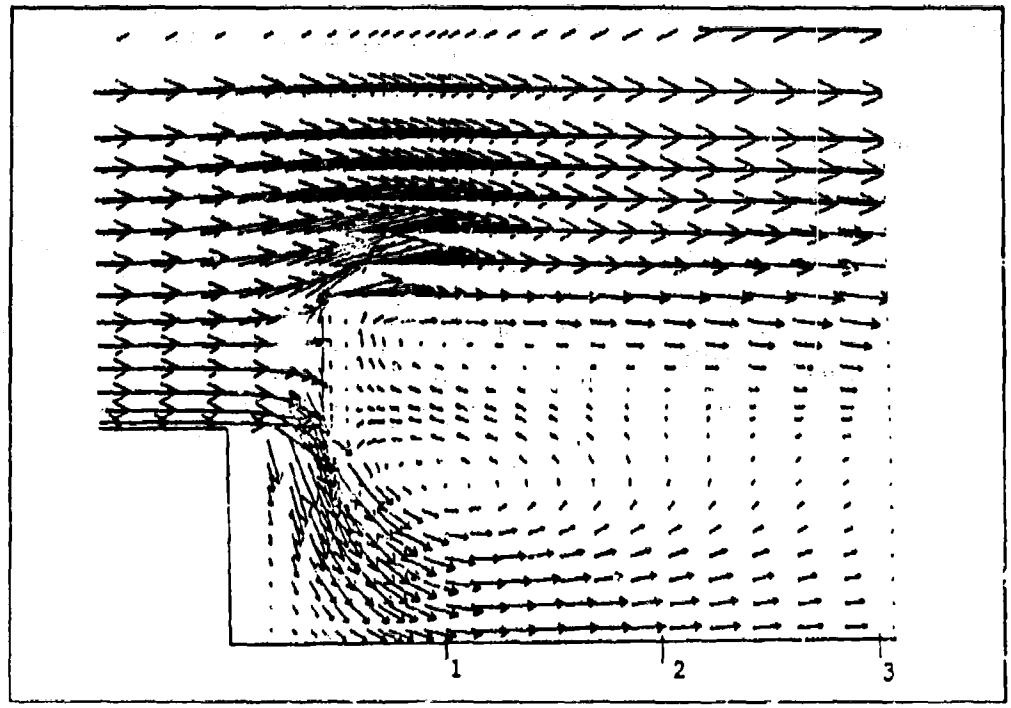

Figure 21. "PHOENICS" Generated Velocity Vector Field for an F50/0%/0/50/0° Deflector [Ref. 1:pp. 54]

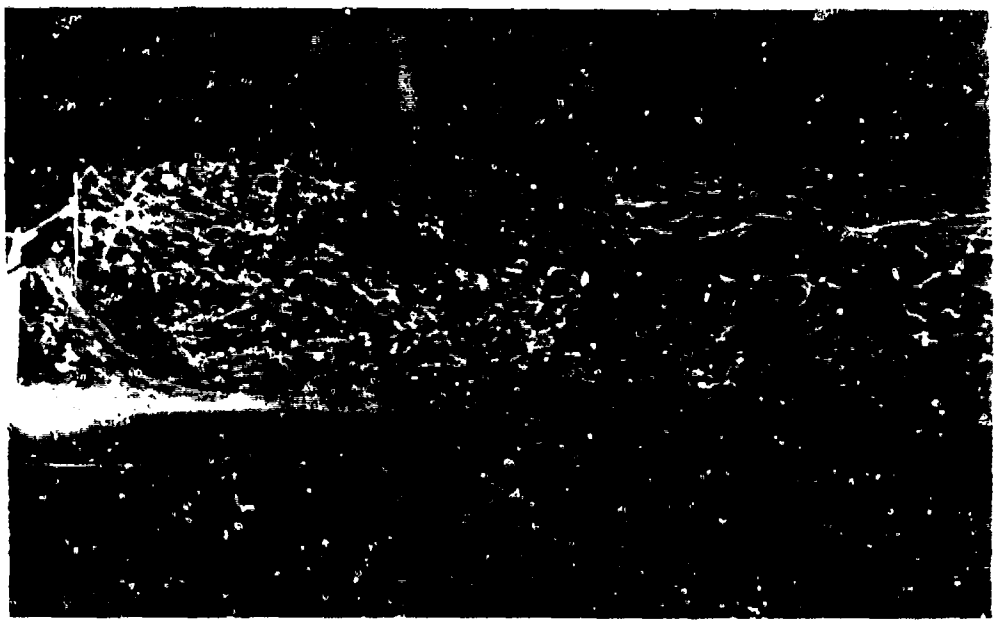

Figure 22. Photograph of an F50/0%/0/50/0° Deflector in the Wind Tunnel

recirculation zone in the lower left hand corner is missing and the recirculation zone is both shorter in the flow direction and centered about one half to three fourths of a step height closer to the step than the actual flow, as recorded in Figure 22. Analysis of the video showed the downstream end of the recirculation zone varied from 2 to 3 H.

Figures 23 and 24 show the results using the F50/0%/0/30/30° deflector. The general S shape of the flow pattern is correct but the location of the recirculation zone is both underpredicted by "PHOENICS" and is smaller and more circular than the actual flow shown in Figure 24. "PHOENICS" also does not predict the small recirculation zone in the lower left hand corner at the base of the step but does predict a second recirculation zone at 2.5 H. This is not evident either in Figure 24 or in the video.

Figures 25 and 26 show the major differences between the "PHOENICS" results and those from the wind tunnel. Both show the results of using an F50/0%/0/12.5/0° deflector. "PHOENICS", in Figure 25, predicts the recirculation zone resulting from the flow down the face of the step to be very small and confined to only one half of a step height downstream. It also predicts a very large recirculation zone centered at about 2.4 H. Figure 26 shows the actual flow to be very different. The recirculation zone at the face of the step is quite large, extending to 2 H horizontally and to the top of the step vertically. The other recirculation zone predicted by "PHOENICS" is present but is not obvious from the photograph in Figure 26. It was seen during video analysis, and extends from about 3 to 6 H. In this case, the downstream position of the

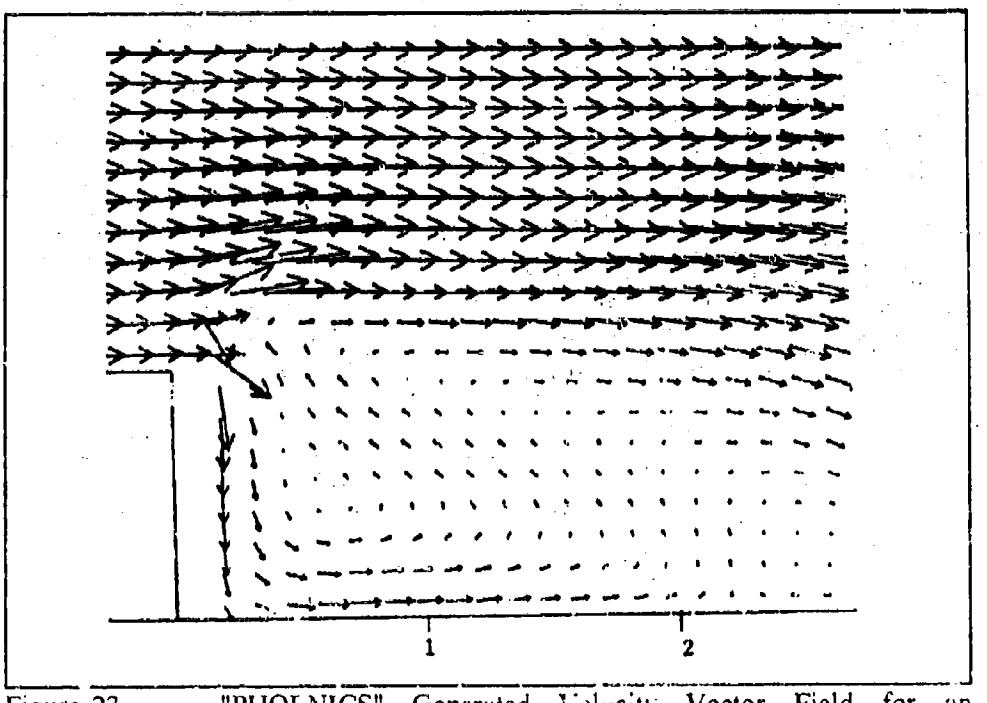

Figure 23. "PHOENICS" Generated Velocity Vector Field for an F50/0%/0/30/30° Deflector [Ref. 1:pp. 58]

Figure 24. F50/0%/0/30/30° Deflector

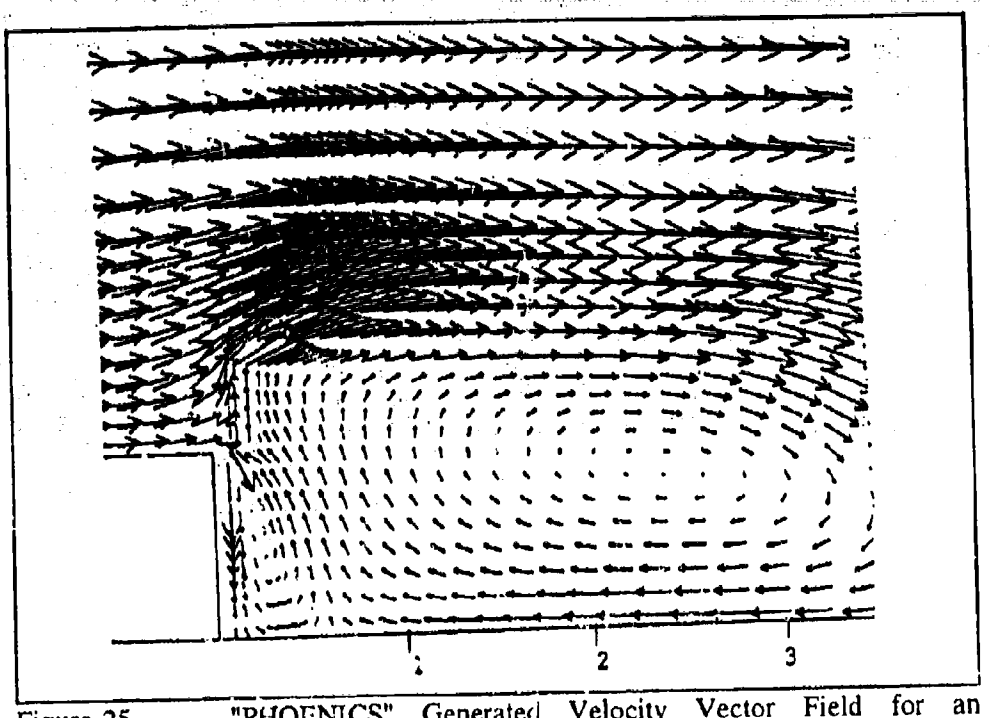

Figure 25. "PHOENICS" Generated Velocity Vector Field for an F50/0%/0/12.5/0° [Ref. 1:pp. 50]

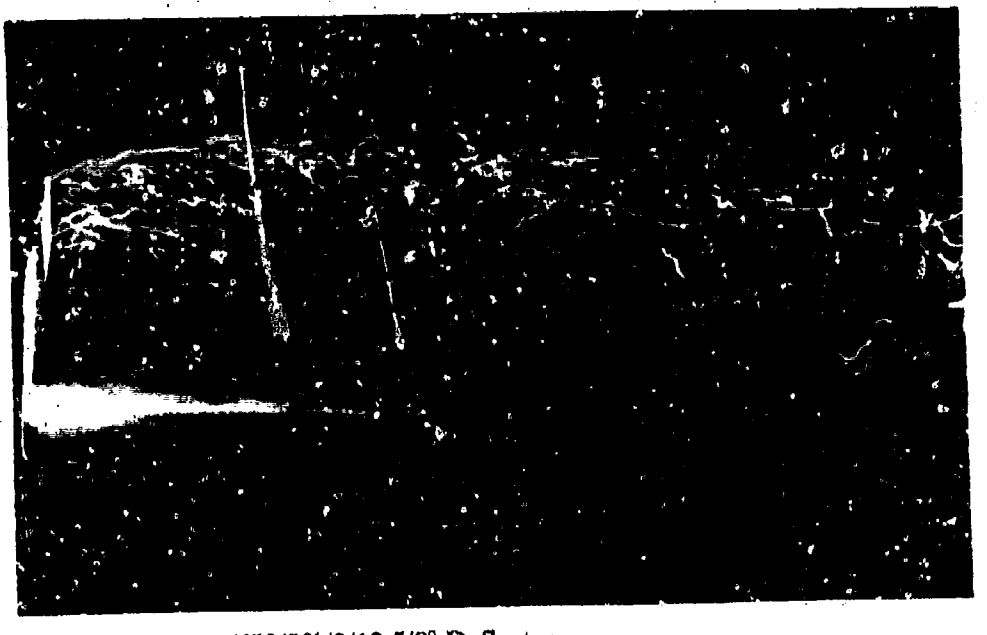

Figure 26. F50/0%/0/12.5/0° Deflector

flow pattern was under predicted by at least two and a half step heights. In general the predicted direction of the flow is incorrect beyond one half step height downstream.

The cause of this discrepancy is not known, but the most likely reason is a grid size in the "PHOENICS" program that is to large, compared to the downstream deflector displacement. This would not allow enough flow through the step to deflector offset to produce the large recirculating zone that was observed experimentally. Reexamining Figures 19-26 reveals that the closer the deflector was to the step the poorer the agreement between "PHOENICS" predicted flow patterns and experimental results. Unfortunately, the grid sizes used were not clearly documented, so no firm conclusions can be drawn until further investigation is conducted; this should be completed if "PHOENICS" is to be used for this project, because the large difference casts doubt on the reliability of its predictions.

A direct comparison between porous deflectors could not be made because Woolman only considered deflectors up to 15% and no deflectors with that small a porosity were available for this study. Woolman stated that for a fence, the recirculation zone was eliminated by 20% porosity while the cited literature indicated it should exist until 30% [Ref. 1:pp. 41]. This would lead one to believe there might be a problem with the porosity function in "PHOENICS". It is also possible that the source of this discrepancy is the same as that of the flow-pattern.

B. FLAT NON-POROUS DEFLECTORS

1. Vertical Deflectors

Non-porous vertical deflectors, of all the available sizes, were run with various orientations. Figures 22 and 26 were fairly typical of the flow patterns for all the deflector sizes. All showed very strong recirculation zones extending to about 1.5 to 2 H. The closer the deflector was to the step, the shorter the recirculation zone, and the smaller the deflector, the lower the shear layer between the clockwise recirculation zone at the top of the deflector and the counterclockwise recirculation zone on the floor. All of these deflectors had a pronounced affect on the flow pattern, but none had the desirable effect of providing a steady flow of constant direction and of low turbulence in the area of interest.

2. 30 Degree Deflectors

The 50 and 38 millimeter deflectors produced similar results at all positions. Figures 27 (repeat of Figure 24) and 28 show each deflector at 30 millimeters. Both produced an S shaped pattern with strong downward velocities going from the deflector to about 1 H. The lower recirculation zone extended out to about 2.5 to 3 H. The smaller deflector had the longer, lower recirculation zone. In both cases the length of the recirculation zone was related to the distance of the deflector from the step. The closer the deflector, the shorter and deeper the zone; deeper meaning a greater vertical dimension. Neither of these deflectors produced desirable results in the area of interest. Analyzing the video revealed the velocity at about 12 millimeters above the floor in the

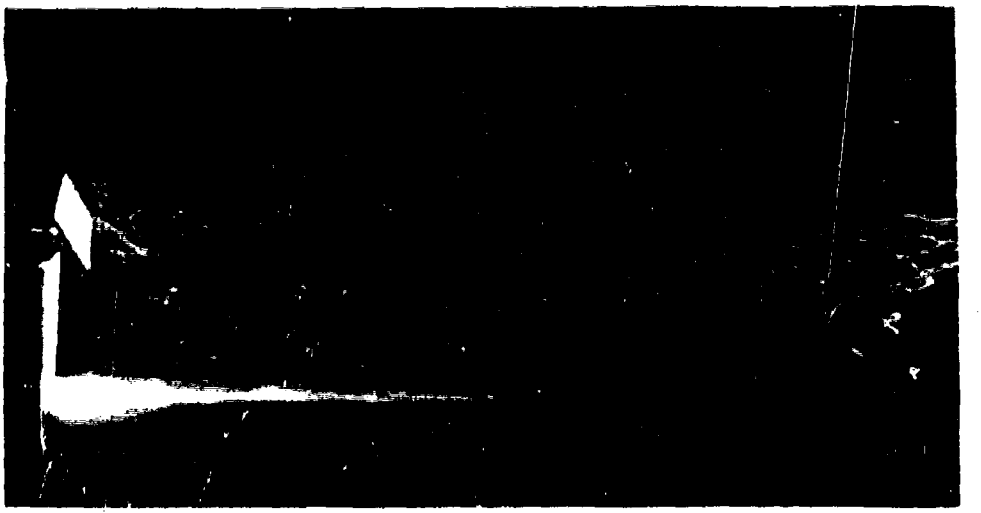

Figure 27. F50/0%/0/30/30° Deflector

Figure 28. F38/0%/0/30/30° Deflector

recirculation zone to have a velocity, on the order of one half the velocity of the flow over the top of the deflector.

The flow around the 25 millimeter deflector proved to be much more dependent, than the 38 millimeter deflectors, on position. For the middle displacements

of 25 and 38 millimeters, the flow resembled that of the 50 and 38 millimeter deflectors, but with not as pronounced a recirculation zone, as shown in Figures 29 and 30. The other displacements produced much different results. Figure 31 and the video show, for the 25 millimeter deflector at 50 millimeter offset, the S shaped flow pattern was completely missing. The deflector was now acting as a bluff body, almost independently of the step. The video revealed that not enough flow was being forced around the bottom edge of the deflector to produce the S pattern flow, but it did seem to effectively reduce the step height, producing a large clockwise recirculation zone beneath the separated flow, resembling a step of reduced height. In the case of the 25 millimeter deflector at 12.5 millimeters offset, the flow around the lower edge was greatly reduced as compared to the 50 millimeter offset. Figure 32 shows a separated

Figure 29. F25/0%/0/38/30° Deflector

Figure 30. F25/0%/0/25/30° Deflector

Figure 31. F25/0%/0/50/30° Deflector

region behind the deflector and a recirculation zone directly beneath it. Neither of these positions improved on the open step, but did seem to indicate that a flat deflector on the order of 10% of step height should be positioned between one half and two deflector widths downstream of the step.

Figure 32. F25/0%/0/12.5/30° Deflector

3. 45 Degree Deflectors

The 50 millimeter deflectors at 45° showed the same basic flow pattern as those placed at 30°. The only difference was the length of the recirculation zone. It was slightly longer in the flow direction and not as deep, as shown in Figure 33. The relationship between the deflector position and the recirculation zone size remains the same as for the 30° deflectors.

The 38 millimeters deflectors gave quite different results at 45° than at 30°. Figure 34 shows the results of the 30 millimeters offset. It shows the separated flow behind the deflector and a weak recirculation zone beneath it. The flow in this recirculation zone displayed higher frequency turbulence on the video than for the 30

Figure 33. F50/0%/0/30/45° Deflector

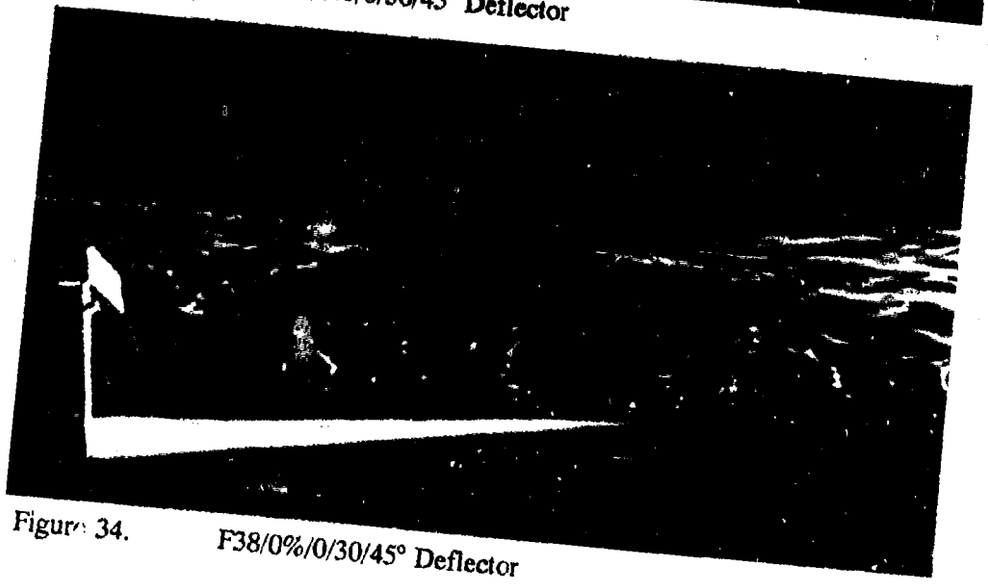

Figure 34. F38/0%/0/30/45° Deflector

degree deflector case. It was evidenced by the bubbles oscillating vertically as they moved horizontally. Figure 35 shows the results at 12.5 millimeters offset. It is not apparent from the figure, but analysis of the video revealed that there is a recirculation

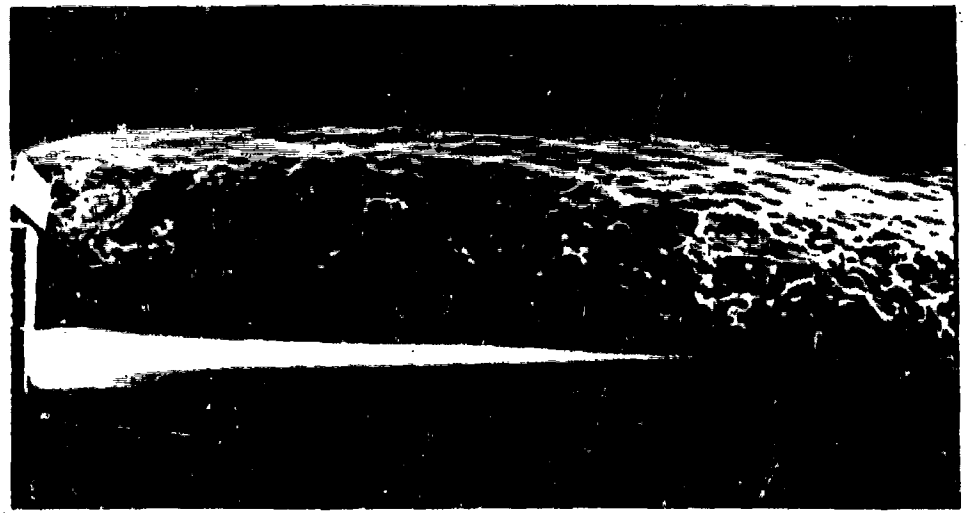

Figure 35. F50/0%/0/12.5/45° Deflector

zone beneath the region separated behind the deflector. It has relatively slow speed flow, but it is quite turbulent,with high frequency fluctuations.

4. Summary

The flat non-porous deflectors have a pronounced effect on the flow patterns behind the step. None of them are particularly desirable for the two dimensional case, but in three dimensions, a very large change in the flow may be desirable. The size and position of the recirculation zone is dependent on deflector placement. The pattern is more stretched out in the flow direction, the farther the deflector is from the step, and small deflectors stop functioning as a deflector, once they are placed closer to the step than one half a deflector width, or further from the step than 2 deflector widths.

C. FLAT POROUS DEFLECTORS

1. Vertical Deflectors

The vertical position at 30 millimeters was used to study the effect of varying porosity on the flow pattern. Deflectors of 42, 46, 48, 51 and 56 percent porosity were available. The 46 through 56 percent porous deflectors all had round holes with a diameter small compared to the deflector width. The ratios of hole diameters to deflector widths are given in Table IV. The 42 percent porous deflector is not listed because it had slots instead of holes. The slots were 6X30 millimeters with rounded ends. Two deflectors of this porosity were used; a 38 millimeter one with vertical slots and a 32 millimeter one with horizontal slots.

The 30 millimeter position was used to study the effects of the varying hole size and shape. Figures 36 and 37 show the results for the 42 percent porous deflector. The flow patterns are essentially identical despite the difference in deflector width. The orientation of the slots vertically or horizontally did not change the resulting pattern. There was no pronounced reattachment zone, but there was a weak recirculation zone extending from the step to about 2 or 2.5 H and to about .8 H vertically. The flow in the recirculation zone was moving at about the same speed, but had more turbulence than the open step, judging from frame to frame movement of the bubbles, when viewed on video tape.

The 30 millimeter position was also used to compare the effects of the other porosities. It was interesting to note from Figure 38 that the 46 percent deflector flow

TABLE IV. Deflector Porosity Details, Hole Diameter to Deflector Width Ratio

Deflector Porosity				
Deflector width	46 mm	48 mm	51 mm	56 mm
38 mm	7.8%	7.8%	6.6%	10.5%
25 mm	11 8%	11.8%	9.8%	15.7%

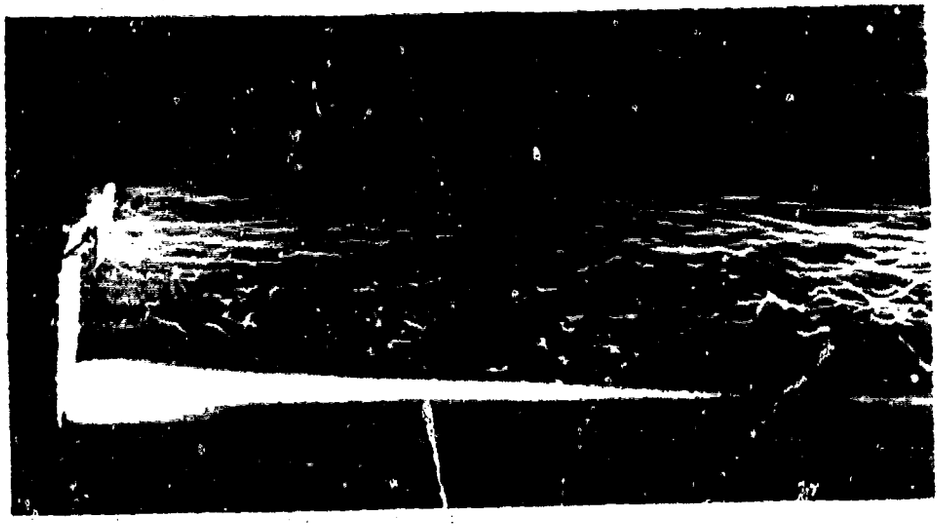

Figure 36. F38/42%/0/30/0° Deflector

pattern was similar to the nonporous pattern pictured in Figure 22, in that it deflected the flow downward and had a small recirculation zone at the base of the step and produced an S pattern flow, though weaker than the nonporous case. It was, however, without the separated flow behind the deflector and, therefore, without the turbulent shear layer that was typical of the S flow pattern in the nonporous cases. This lower

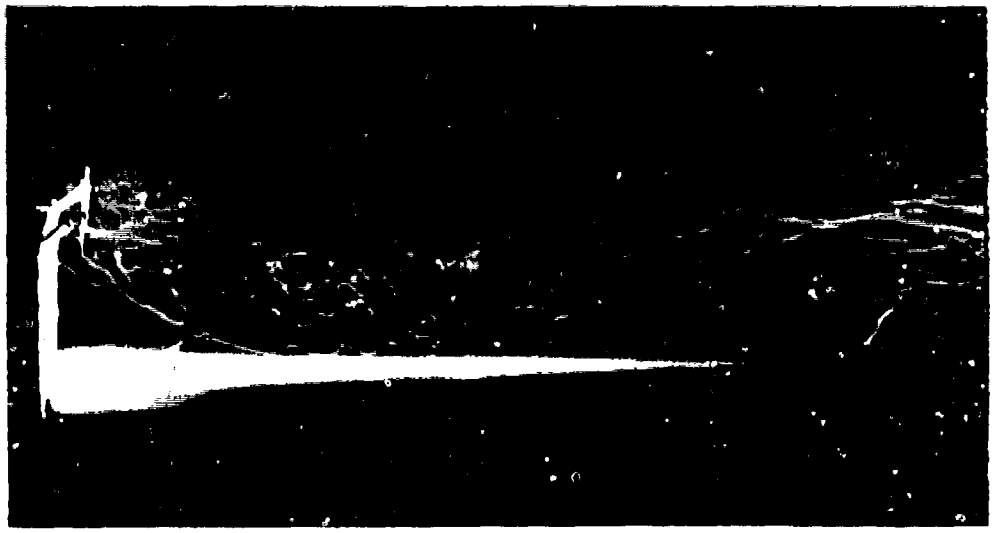

Figure 37. F32/42%/0/30/0° Deflector

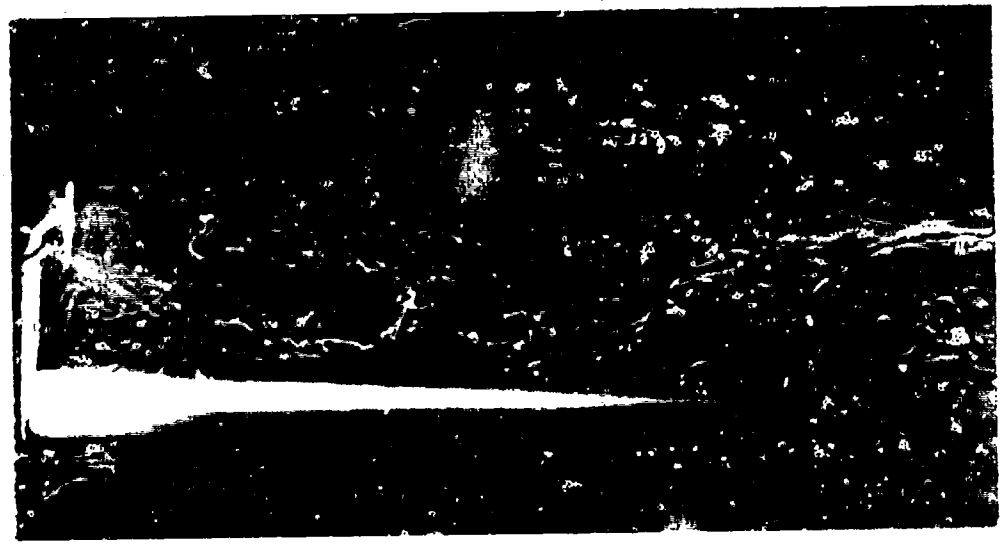

Figure 38. F38/46%/0/30/0° Deflector

apparent turbulence intensity made the flow pattern more desirable than the open step case, but still failed to achieve uniformity of flow in the region of interest.

Figures 39 and 40 show the results for the 48 and 56 percent porous cases respectively which were also similar to the 51 percent case. The flow patterns are very

Figure 39. F38/48%/0/30/0° Deflector

Figure 40. F38/56%/0/30/0° Deflector

similar, even though the 56 percent deflector had a higher hole diameter to width ratio. The flow in Figures 39 and 40 exhibit a weak recirculation zone from the step to about 2 H. From the video, the velocity appeared to be about one fourth of that over the top of the deflector. The turbulence intensity appears to be between those of the 42 percent

deflector and the open step. The effect of moving the 38 millimeter deflector closer to the step can be seen in Figure 41. While it was not obvious from the figure, the video reveals a weak recirculation zone extending to about 2.5 H. The flow within it was lower in velocity and turbulence than resulted for larger deflector to step separations. This is the first flow that shows relatively uniform flow within the area of interest.

The 25 millimeter deflectors produced essentially the same flow pattern as the 38 millimeter ones. Figure 42 shows that the 51 percent porous deflector produced a pattern similar to the 48 and 56 percent, 38 millimeter deflector used for Figures 38 and 40. All show a recirculation zone extending to about 2 H. The video revealed the velocities and turbulence levels to be about equal in all the cited cases.

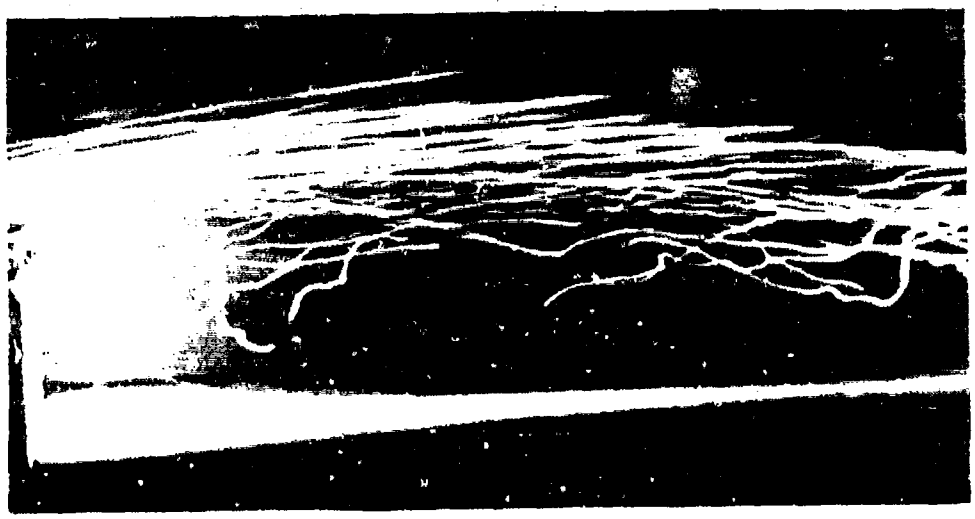

Figure 41. F38/48%/0/12.5/0° Deflector

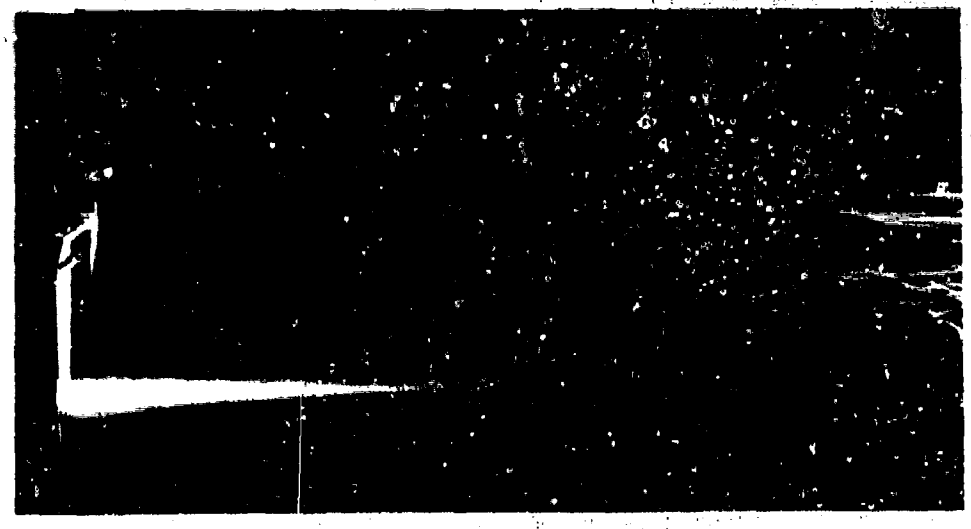

Figure 42. F25/51%/0/25/0° Deflector

2. 30 Degree deflectors

The whole series of porosities were again run at the 30 degree and 30 millimeters offset to evaluate the effect of changing porosities of the angled deflectors. The results were what would be expected; the flow was not substantially different from that of the same deflector at 0 degrees. The main difference was in the length of the recirculation zone, which was slightly longer for the 30 degree case, as can be seen by comparing Figure 43 and 38; in both cases, the deflector was 46 percent porous. The video revealed the recirculation zone velocities to be approximately equal for all the cases. Changing the offset distance of the deflector did change the resulting pattern. Moving the deflector closer to the step, resulted in a less pronounced recirculation zone as can be seen in Figures 44, 45 and 46, which corresponds to the 48 percent porous

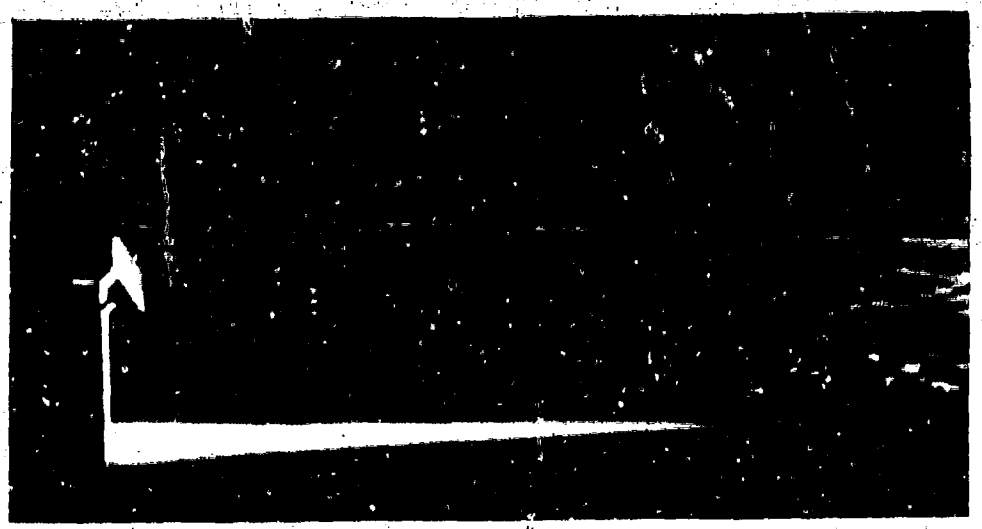

Figure 43. F38/46%/0/30/30° Deflector

Figure 44. F38/48%/0/12.5/30° Deflector

deflector at 12.5, 25 and 30 millimeters respectively. Although the figures do not show it, the video revealed the velocities to be similar, but the 12.5 millimeter offset had a much more high frequency turbulence in the recirculation zone, as evidenced by the oscillating bubble paths. Reducing the deflector size had a larger effect on the flow

Figure 45. F38/48%/0/25/30° Deflector

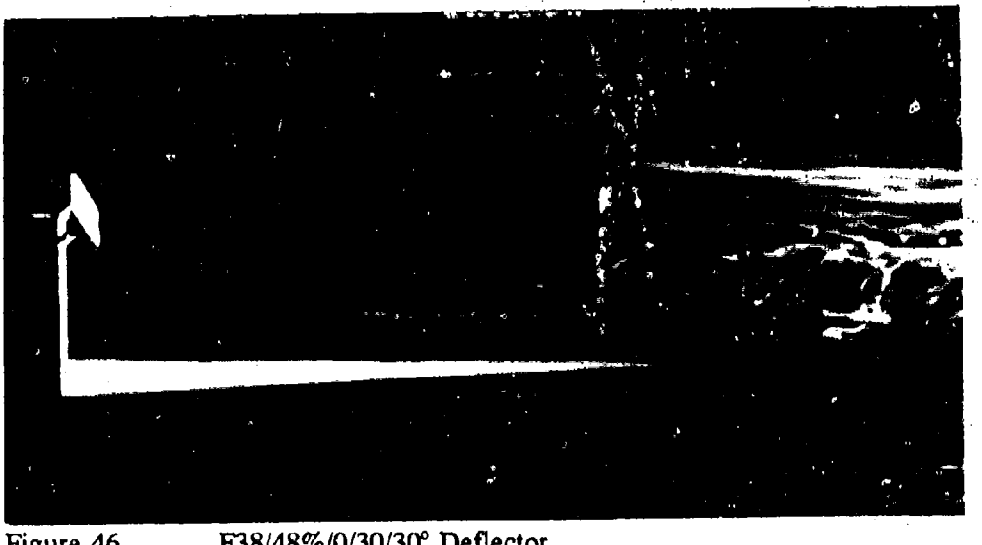

Figure 46. F38/48%/0/30/30° Deflector

pattern here than it did in the vertical deflector case. The 25 millimeter, 51 percent, deflector was placed at 38, 25 and 12.5 millimeters as shown in Figures 47 through 49. These figures show that, as the deflector is moved closer to the step, the strength of the recirculation zone at the base of the step decreases and the vertical depth increases until

Figure 47. F25/51%/0/38/30° Deflector

Figure 48. F25/51%/0/25/30° Deflector

at 12.5 millimeters it disappears altogether and is replaced by a much larger slower recirculation zone extending from the step to 3 to 4 H. This large recirculation zone is not evident in Figure 49 but was seen on the video. The turbulent shear layer at the top of the recirculation zone is evident in Figure 49, but was not steady in its vertical

Figure 49. F25/51%/0/12.5/30° Deflector

position relative to the step. Except for this unsteady shear layer, this position/deflector combination produced a relatively constant upward flow in the area of interest.

3. 45 Degree Deflectors

Only 38 millimeter deflectors were positioned at 45 degrees and they produced results essentially the same as the 25 millimeter deflectors at 30 degrees. One factor in this similarity was the reduction of the effective vertical area and porosity of the deflector by the cosine of the given angle. Comparison of Figures 49 and 50 illustrate the similarity.

4. Negative-Angle Deflectors

Almost as an after-thought, the 48 percent deflector was placed at a negative angle of 35 and 60 degrees with the lower edge of the deflector resting on the step corner. This position deflected the flow upward instead of down. The resulting pattern

Figure 50. F38/48%/0/12.5/45° Deflector

can be seen in Figure 51 and 52. Neither flow resulted in enough bubbles entering the recirculation zone to reveal what was happening, so bubbles were injected at 6 H on the floor toward the step. The minus 35 degree position resulted in a reattachment zone at about 7 H, and for the minus 60 degree position, it was about 6 H. Both resulted in a single large recirculation zone, extending from the step to the reattachment zone. The flow in this region was less visibly turbulent than for any other deflector position and with a velocity at about 12 millimeter off the floor of about 30 percent of flow velocity over the top of the deflector.

5. Summary

In all positions, the porous and nonporous deflectors had dramatically different effects on the flow pattern. In almost all cases, the porous ones were superior in terms of providing a moderately uniform, low turbulent flow in the area of interest.

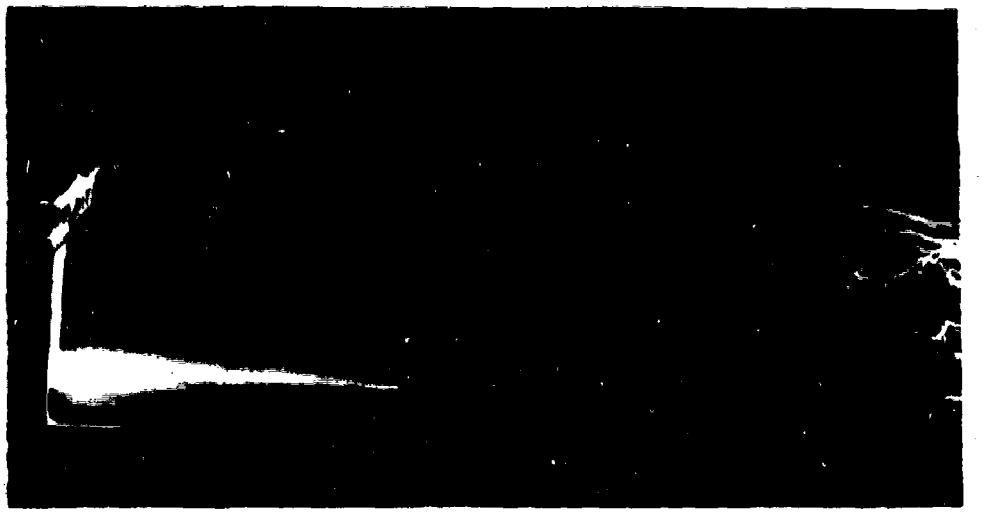

Figure 51. F38/48%/0/0/-35° Deflector

Figure 52. F38/48%/0/0/-60° Deflector

The best flow, in terms of the area of interest, resulted from the negative-angle positions, followed by the vertical positions.

D. CURVED DEFLECTORS

All curved deflectors were nonporous circular arc segments. Two arc lengths and four radii of curvature were available as listed in Table V. The 90 degree arc deflectors were always positioned so the tangent to the leading edge was parallel to the oncoming flow and the tangent to the trailing edge was vertical. For the 60 degree arc deflectors, the trailing edge tangent angle to the vertical was used to define the deflector position. The configuration is shown in Fig 18 and three angles were used: 0, 15 and 30 degrees. In the following discussion, the deflectors are referred to by arc-length in degrees and radius of curvature in millimeters, without specific labels as such.

1. 90 Degree Arc Length

The results of the 57 and 44 millimeter deflectors are included for completeness, but are impractically large at 71 and 55 percent of H respectively.

Figures 53 and 54 show the dramatic affect of the 57 and 44 millimeter deflectors had on the flow. They were positioned at 25 millimeters and 12.5 millimeters offset respectively. Both display the familiar S flow that was seen in the flat nonporous deflectors. The major difference from the flat deflectors, is the absence of the separated region behind the deflector and the resulting turbulent shear layer.

TABLE V. Circular Arc Deflectors

Arc Length	Radius of Curvature			
90°	57 mm	44 mm	28 mm	12 mm
60°	57 mm	44 mm	28 mm	N/A

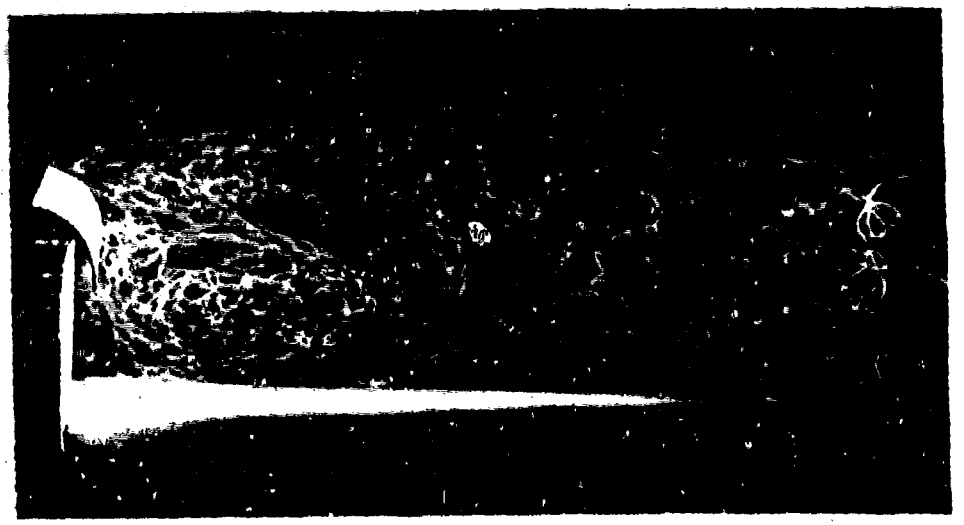

Figure 53. C90/57/0/25/0° Deflector

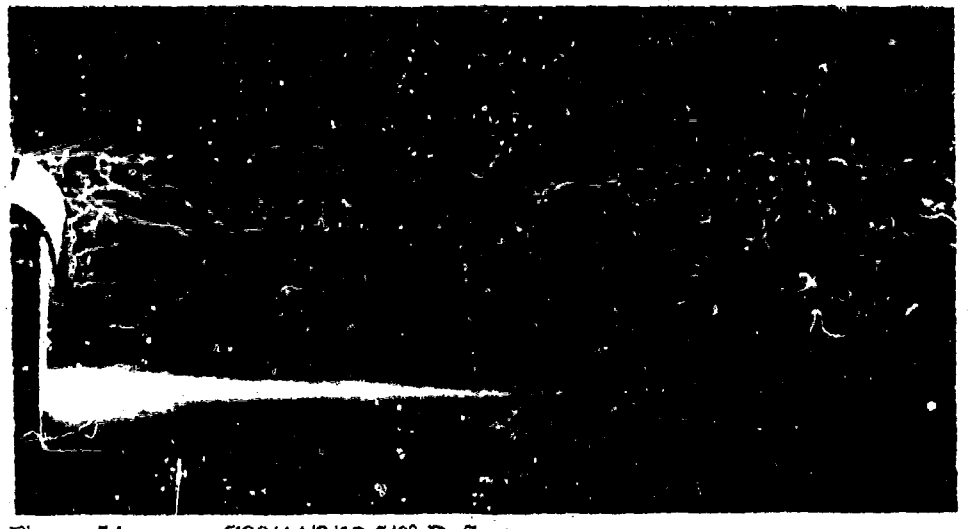

Figure 54. C90/44/0/12.5/0° Deflector

The only position for the 12 millimeter deflector, that did not result in separated flow behind it, was at 25 millimeters as shown in Figure 55. The pattern is basically similar to the flow from the flat, nonporous, 25 millimeter wide deflector pictured in Figure 49. The recirculation zone was shallower vertically and a little

Figure 55. C90/12/0/25/0° Deflector

longer horizontally, but considering the 12 millimeter curved deflector was equivalent to only a 17 millimeter flat deflector at 45 degrees, in flow intercept area, the magnitude of the effect on the flow is large.

Figure 56 is the result of positioning the 28 millimeter deflector at 12.5 millimeters offset. The flow pattern resembles the flow from the flat, nonporous, 50 millimeter deflector placed at 12.5 millimeters, as shown in Figure 26. The main difference in patterns is that the curved deflector's recirculation zone is not as vertically deep as the flat deflector's. This is probably the result of the curved deflector's smaller vertical displacement resulting in smaller vertical disturbance of the flow.

The flow resulting from placing the 28 millimeter deflector at 25 millimeters offset is shown in Figure 57. It shows the familiar S pattern of flow and resembles the flow of the flat, nonporous, 50 millimeter at 25 millimeters offset and 30 degrees angle.

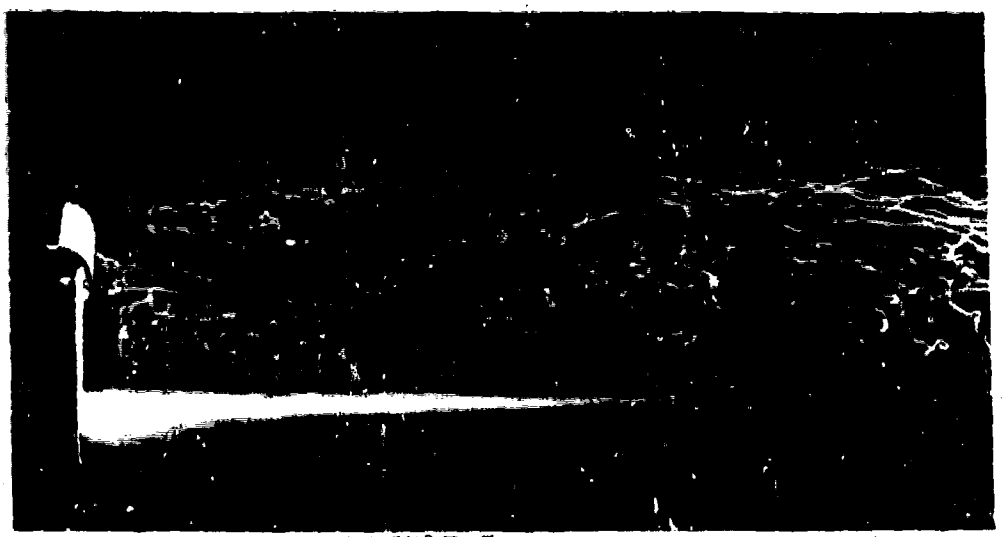

Figure 56. C90/28/0/12.5/0° Deflector

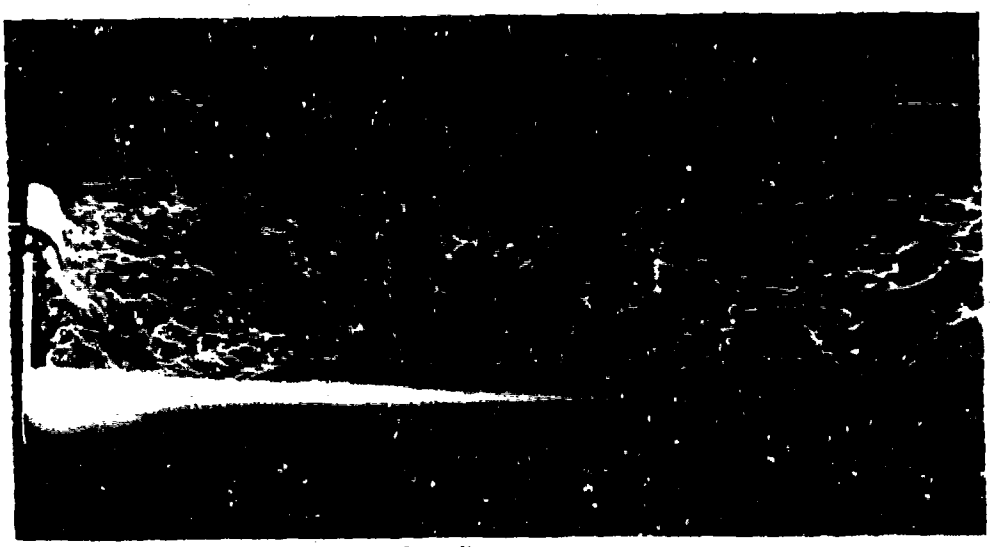

Figure 57. C90/28/0/25/0° Deflector

2. 60 Degree Arc Deflectors

Only the 44 and 28 millimeter 60 degree arc deflectors were used. First the effect of offset was studied at the 0° position. Figure 58 shows the separated flow

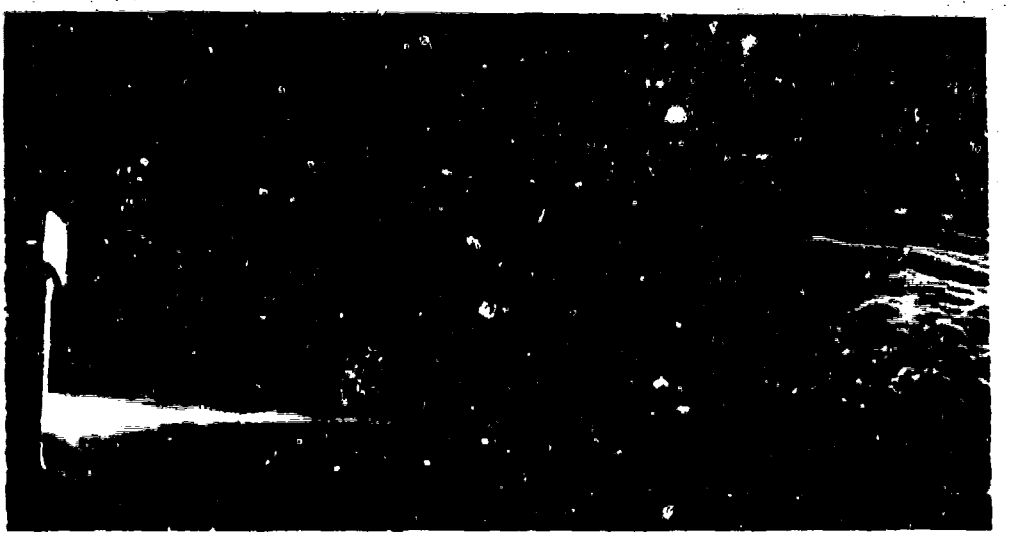

Figure 58. C60/28/0/12.5/0° Deflector

region behind the deflector, with the reattachment zone at about 6 H. The recirculation zone in Figure 58, immediately below the deflector was revealed, by the video, to be very unsteady. Most of the time a large clockwise recirculation zone existed between the step and the reattachment region, but every few seconds, a small counter clockwise eddy would burst down from the deflector. This is what appears in the photograph in Figure 58.

Figures 59 and 60 show the result of moving the deflector to 25 and 38 millimeters respectively. Both show the same type of S shaped flow pattern that was seen in the flat nonporous deflectors. They also display the same relationship of recirculation zone length to offset distance which is the greater the offset, the greater the recirculation zone length.

Figure 59. C60/28/0/25/0° Deflector

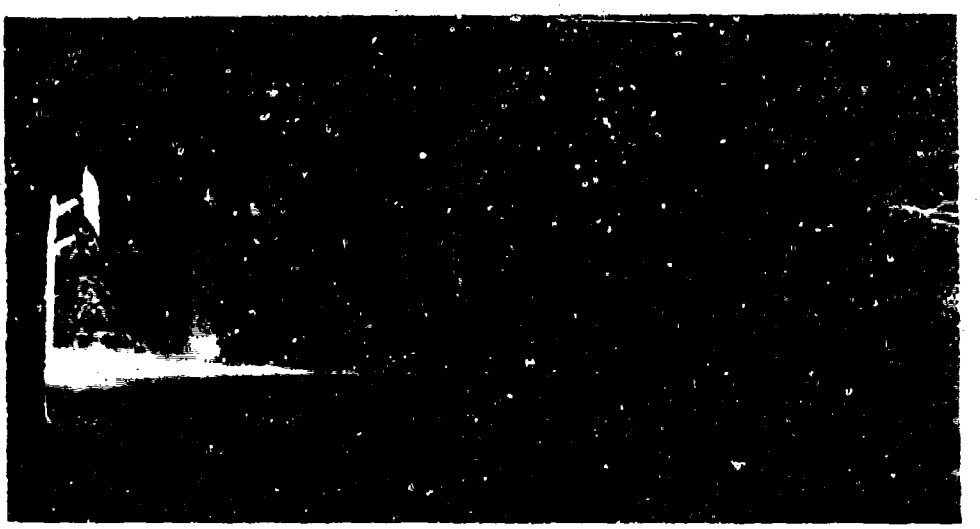

Figure 60. C60/28/0/38/0° Deflector

Figure 61 shows that the 44 millimeter deflector, placed at 12.5 millimeters, produces the basic S pattern of flow. The resulting flow again resembles the flat nonporous deflector flow of Figure 26. Figure 62 demonstrates the same relationship

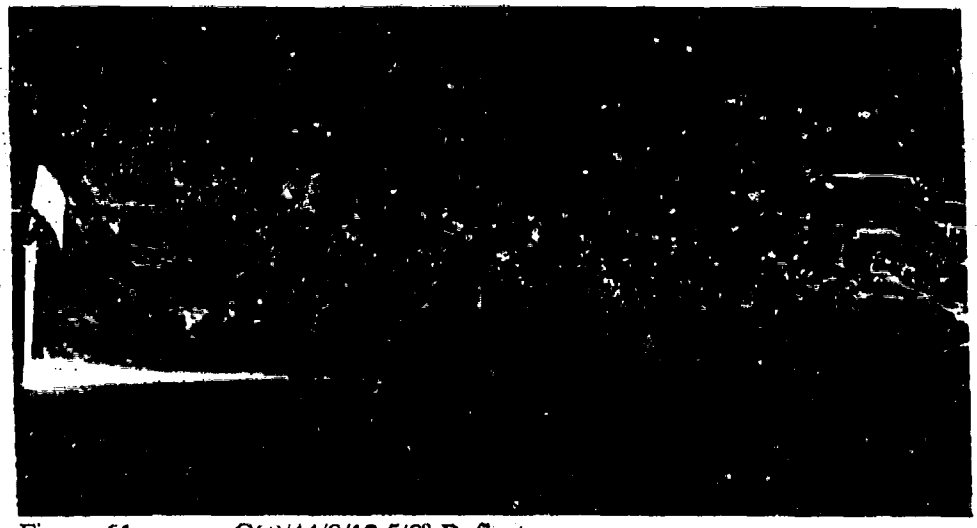

Figure 61. C60/44/0/12.5/0° Deflector

Figure 62. C60/44/0/38/0° Deflector

of flow pattern due to deflector placement as described above, except with a clockwise recirculation zone at the base of the step.

The last aspect of the curved deflectors studied was the effect of varying the downstream angle at 25 millimeters offset. Each deflector was positioned with an angle

of 15 and 30 degrees, with the results for the 28 millimeter deflector shown in Figures 63 and 64 respectively. Figure 63 shows a recirculation zone extending to about 2 H, with separated flow behind the deflector, and a region of high turbulence between 1 and 2 H downstream from the step. Figure 64 shows the reattachment zone to be about 4 H from the step, for the 30 degree angle position. The turbulence in the area of interest is lower than for the 15 degree case but was still higher than for the open step.

The 44 millimeter deflector, when placed in the 30 degree position, Figure 65, exhibited results similar to the 28 millimeter deflector pictured in Figure 63 and 64. The reattachment zone is in the same 4 H region with similar separated flow behind the deflector. The major difference was that the shear layer extended almost to the floor, making the flow in the area of interest very turbulent. The 15 degree case is pictured

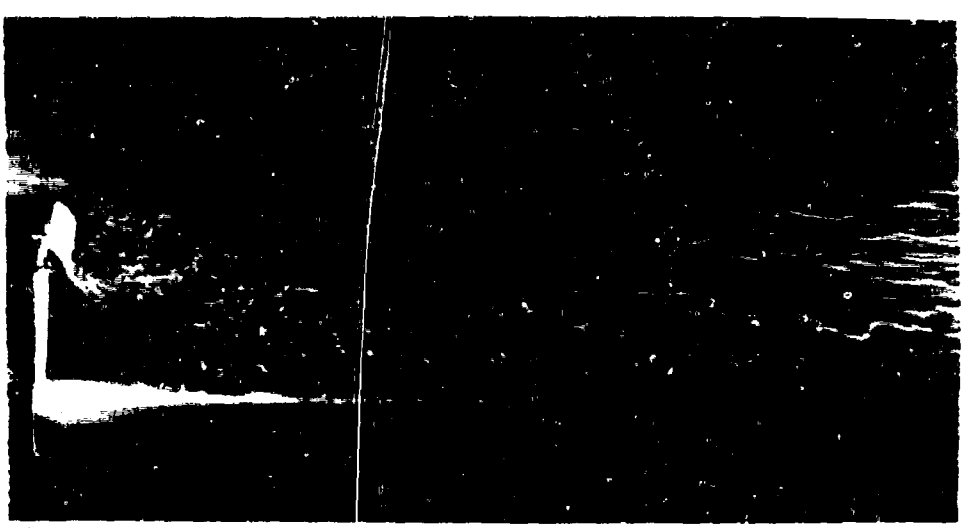

Figure 63. C60/28/0/25/15° Deflector

Figure 64. C60/28/0/25/30° Deflector

in Figure 66. The flow shows the same S shape that was seen before, but the reattachment zone is moved out, compared with the 0 degree case.

3. Summary

In general, the curved deflectors had an effect on the flow similar to the flat, relatively narrow, nonporous deflectors. As in the case of the flat nonporous deflectors, none of the nonporous curved deflectors gave good results in the area of interest.

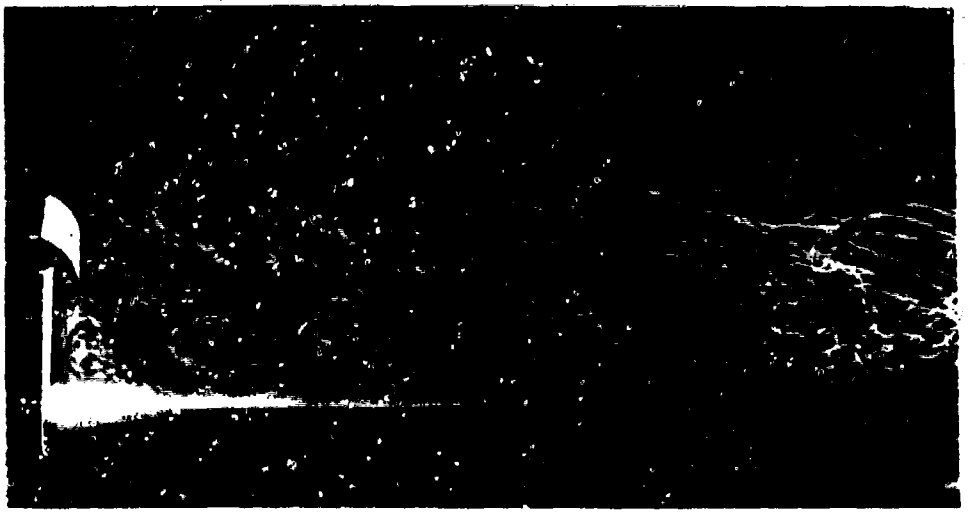

Figure 65. C60/44/0/25/30° Deflector

Figure 66. C60/44/0/25/15° Deflector

VI. CONCLUSIONS AND RECOMMENDATIONS

The initial goals of this study were to:

1. Validate the results of the previous study of this problem using the "PHOENICS" Computational Fluid Dynamics program.
2. Determine if the flow over a two-dimensional backward facing step can be modified in a beneficial way, by reducing the velocity and the turbulence levels.
3. If the answer to number two is in the affirmative, then determine a deflector shape, position and porosity to achieve this flow.

"PHOENICS" produced good results for the open step, but underpredicted the length of the downstream flow pattern, as expected. It did not do as well when a deflector was added. The underprediction grew larger as the offset of the deflector grew smaller. The "PHOENICS" program appears to be very useful, so long as the deflector is positioned fairly far away from the step. For the cases studied, this means at least twenty four percent of the step height. The source of this problem could lie in the grid size chosen. Before relying on the predictions of "PHOENICS", for any further studies, this problem should be investigated. The maximum grid size should be determined, that will allow the use of the largest grid size possible for each problem, thus minimizing the computation time required, while maximizing the confidence in the answer obtained.

Almost any of the figures in this study confirm the modifiability of the flow over the backward facing step. Given a large enough deflector, the flow pattern could be radically changed. A casual look at these same figures leads to the conclusion that the flow pattern could be made much worse, if the correct deflector and position was not chosen; being able simply to modify the flow is not enough.

Finding the best deflector and position out of the infinite possibilities proved not to be possible. However, a few possibilities were discovered along with some general guides as to the choice of deflector/position combinations.

1. The nonporous flat and curved deflectors had a large effect on the flow pattern, but also tended to introduce a large amount of turbulence due to the separated flow behind the deflector and the resulting shear layer.

2. The curved deflectors produced a larger effect on the flow relative to their size, than the flat nonporous deflectors while introducing somewhat less turbulence.

3. When the deflector is large enough to produce a counterclockwise recirculation zone, the downstream length of this zone is roughly directly proportional to the offset distance of the deflector.

4. Porous deflectors produced much less radical changes in the flow pattern, but also introduced much less turbulence.

5. The best flow pattern found for the two-dimensional case was a 48 percent porous deflector angled at a negative angle. This arrangement greatly increased the reattachment length, while the porosity allowed flow to enter the area directly behind the deflector, thereby providing a fairly uniform streamwise flow in its wake.

6. Several good flow pattern resulted from a vertical porous deflector, presumably for the same reasons.

7. These flow patterns are not directly applicable to the three-dimensional flow that applies to most ships. Care needs to be exercised in making that application.

It is unlikely that the deflector positions cited as good, for the two-dimensional case would be equally good for the three-dimensional one, but the basic local effect the deflector has on the flow should transfer well.

The above conclusions, considered in conjunction with the probable future direction of this on-going study, lead to the following recommendations for areas of further investigation:

1. The "PHOENICS" CFD program should be thoroughly tested before it is used without experimental verification.

2. The effect of porous curved deflectors should be studied. The porous flat deflectors were an improvement over the nonporous ones and it is possible that a similar improvement will occur for the curved deflectors.

3. Explore the effect of deflectors on three-dimensional flow over a block.

4. Modifying the flow over a forward facing step; simulating the side of the ship.

5. Combine the forward facing step and the block and deflector studies with this backward facing step study into a generic ship study.

6. Analyze the influence of local Reynolds number on the flow patterns.

7. Ultimately, determine what constitutes an ideal non-aviation ship for helicopter operations.

8. Because of the substantial loss in detail in producing the half-tones for the thesis, an improved method should be investigated.

APPENDIX - GRAPHS OF PROCESSED DATA

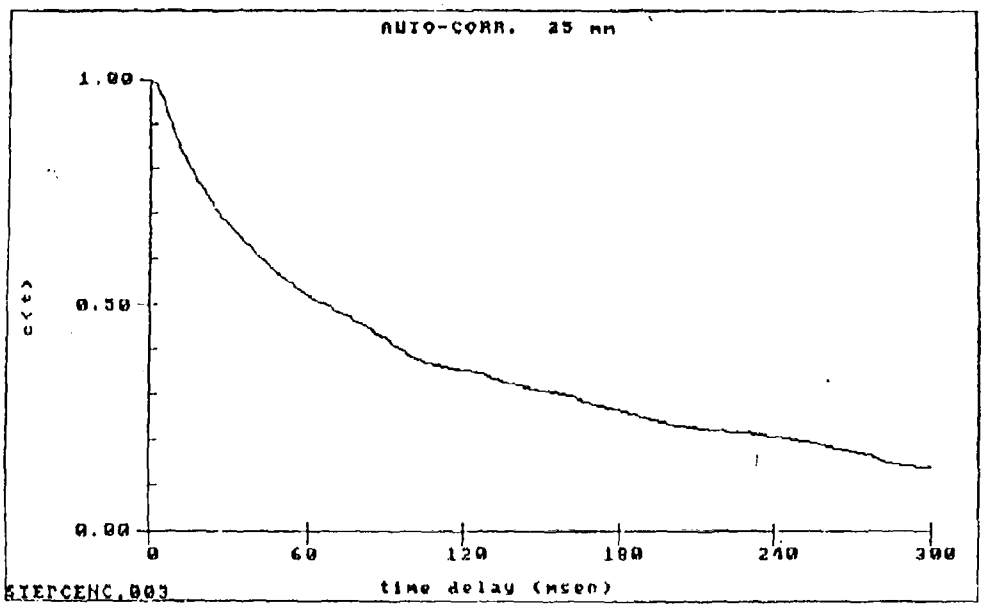

Figure 67. Auto-correlation for the Step Centerline, 25 mm Elevation

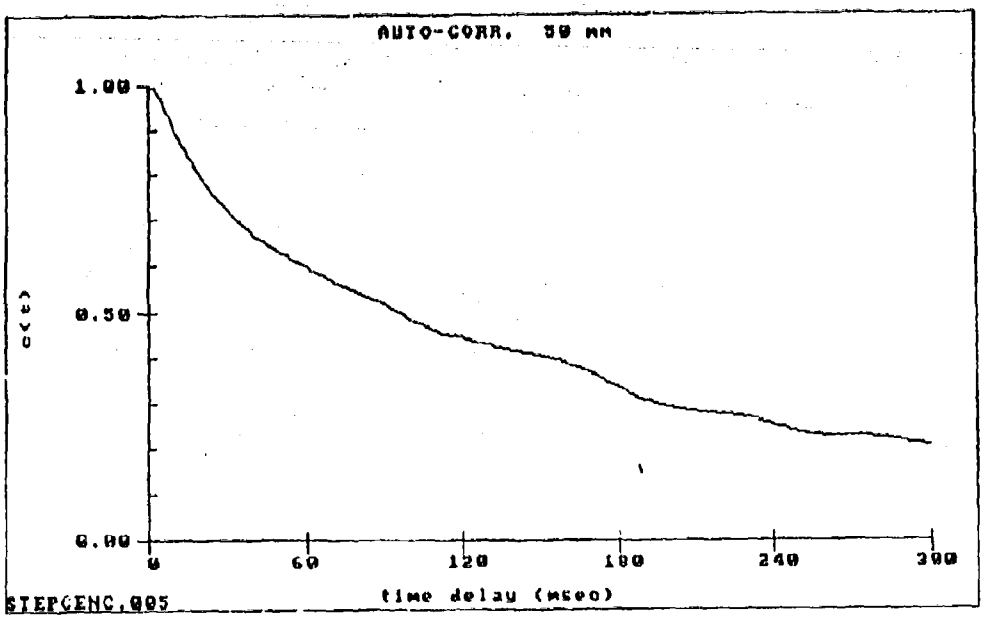

Figure 68. Auto-correlation for the Step Centerline, 50 mm Elevation

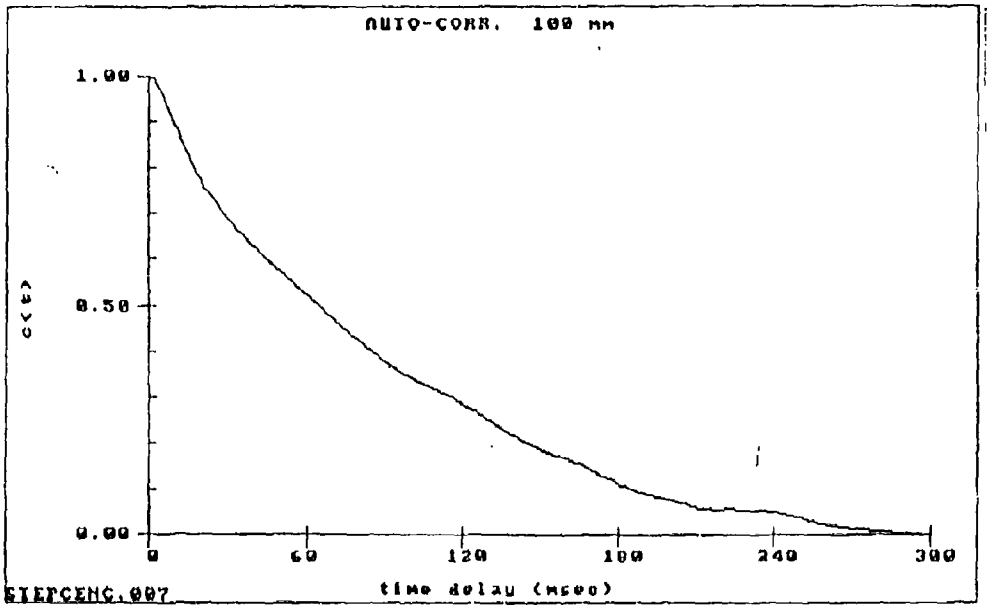

Figure 69. Auto-correlation for the Step Centerline, 100 mm Elevation

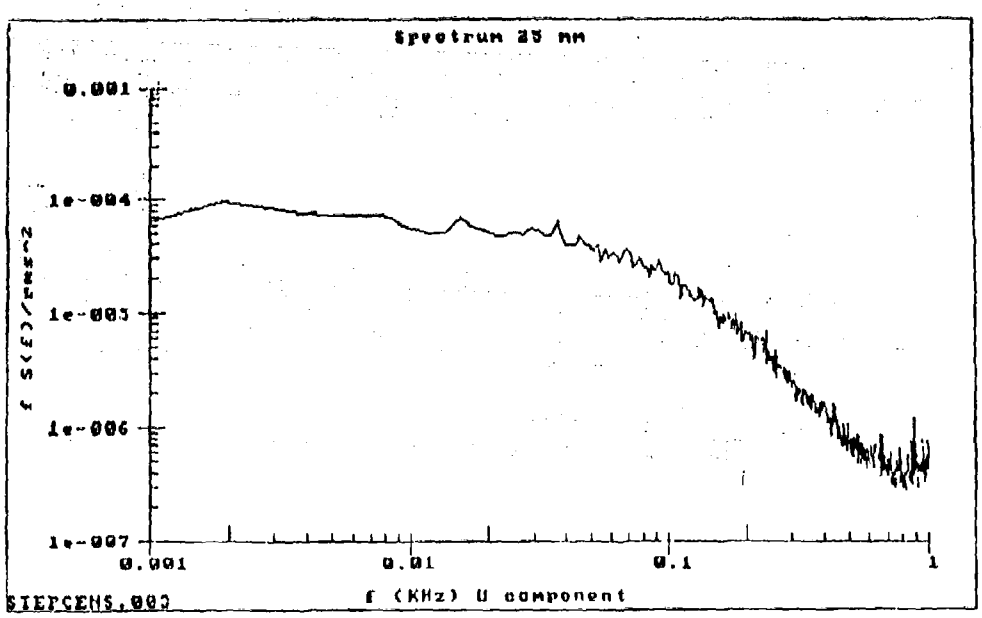

Figure 70. Spectrum Function for the Step Centerline, 25 mm Elevation

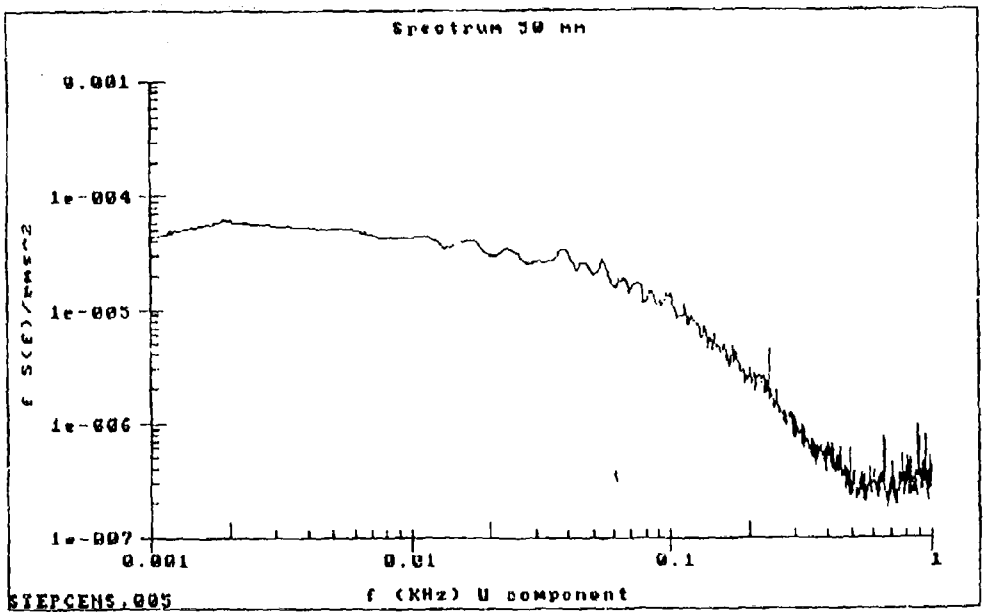

Figure 71. Spectrum Function for the Step Centerline, 50 mm Elevation

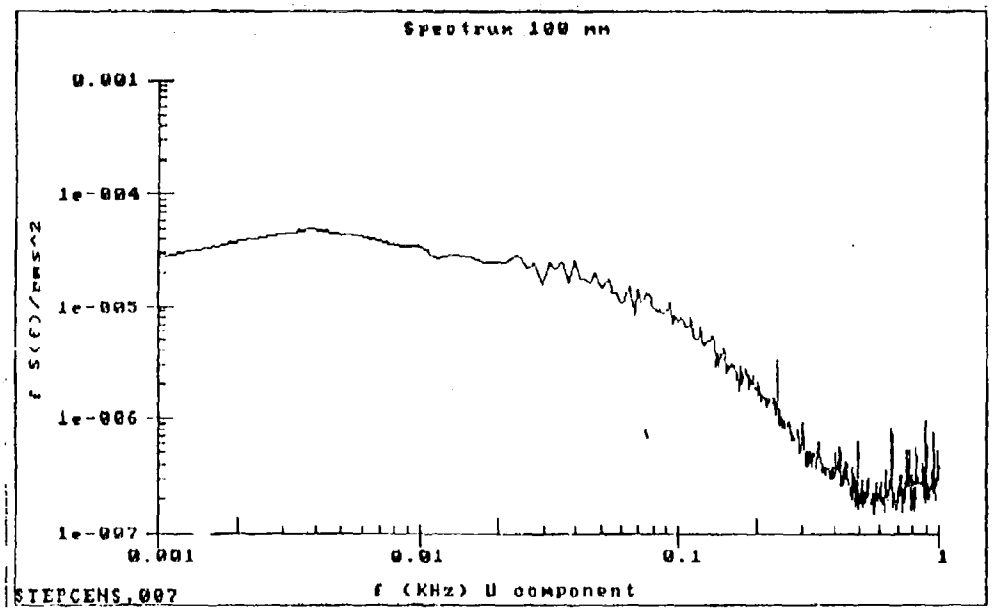

Figure 72. Spectrum Function for the Step Centerline, 100 mm Elevation

LIST OF REFERENCES

1. Woolman, S. G., *Control of Flow Over a Backward Facing Step*, M.S. Thesis, Naval Postgraduate School, Monterey California, September 1990.

2. Naval Air Engineering Center NAEC-ENG-7526 Rev AF, *Shipboard Aviation Facilities Resume*, Department of the Navy, Naval Air Engineering Center, Lakehurst, New Jersey, p.122. April 1988.

3. Naval Warfare Publication (NWP-42 Rev.H), *Shipboard Helicopter Operating Procedures*, Washington, D.C., Department of the Navy, March 1988.

4. Naval Air Test Center Technical Report, *H-46 Dynamic Interface Tests Aboard the USS Missouri (BB-63)*, Department of the Navy Naval Air Test Center, Patuxent River, Maryland, September, 1988, p. 7.

5. Boeing Vertol Company Inter Office Memorandum, *107/H-46 Tunnel Strike Mishap History*, April 1983.

6. Madey, S.L. and L.D. Whitmer, *SH-2F/SH-3F Interface Tests Aboard the USS Ticonderoga (CG-47)*, Naval Air Test Center Report No. RW-14R-83., November, 1984.

7. Healey, J. Val., *Simulating the Helicopter/Ship Interface as an Alternative to Current Methods of Determining Safe Operating Envelopes*, Naval Postgraduate School Report, NPS 67-86-003, Monterey, California, September 1986.

8. Johns, M. K., *Flow Visualization of the Airwake Around a Model of a DD-963 Class Destroyer in a Simulated Atmospheric Boundary Layer*, M.S. Thesis, Naval Postgraduate School, Monterey, California, September 1988.

9. Rhoades, M., *A Study of the Airwake Aerodynamics Over the Flight Deck of an AOR Model Ship*, M.S. Thesis, Naval Postgraduate School, Monterey, California, September 1990.

10. Hunt, J.C.R., C.J. Abell, J.A. Peterka and H. Woo, *Kinematic Studies of the Flows around Free or Surface Mounted Obstacles; applying Topology to Flow Visualization*, Journal of Fluid Mechanics, Vol. 86, 1978, pp. 179, 200.

11. Bearman, P.W., *Vortex Shedding from Bluff Bodies, Annual Review of Fluid Mechanics*, Vol. 16, 1984, pp. 195,222.

12. Peterka, J.A., R.N. Meroney and K.M. Kothari, *Wind Flows About Buildings*, Journal of Wind Engineering and Industrial Aerodynamics, Vol. 21, 1985, pp. 21-38.

13. Woo, H.G.C., J.A. Peterka,and J.E. Cermak, *Wind Tunnel Measurements in the Wakes of Structures*, NASA Contractor Report, NASA CR-2806, 1977.

14. K.M. Kothari, J.A. Peterka and R.N. Meroney, *Stably Stratified Building Wakes*, U.S. NRC Report, NUREG/CR-1247, 1979.

15. Eaton, J.K. and J.P. Johnston, *A Review of Research on Subsonic Turbulent Flow Reattachment*, American Institute of Aeronautics and Astronautics, 80-1438, 1980, pp. 1093-1099.

16. Bradshaw, P. and F.Y. Wong, *The Reattachment and Relaxation of a Turbulent Shear Layer*, Journal of Fluid Mechanics, Vol. 52, 1972, pp.113-135.

17. Goldstein, R.J., V.L. Eriksen and E.R. Eckert, *Laminar Separation, Reattachment, and Transition of Flow over a Downstream-Facing-Step*, Transactions of the ASME, Journal of Basic Engineering, Vol. 92D, No. 4, 1970, pp. 732-741.

18. Eaton, J.K. and J.P. Johnston, *Turbulent Flow Reattachment: an Experimental Study of the Flow and Structure behind a Backward-Facing Step*, Dept. of Mechanical Engineering, Stanford Univ., Rept. MD-37,1978.

19. Atli, V., *Subsonic Flow Over a Two-Dimensional Obstacle Immersed in a Turbulent Boundary Layer on a Flat Surface*, Journal of Wind Engineering and Industrial Aerodynamics, Vol. 31, 1988, pp. 225-239.

20. Sinha, S.N., and A.K. Gupta, *Laminar Separating Flow over Backsteps and Cavities*, American Institute of Aeronautics and Astronautics, Vol. 20, 1982, pp. 370-375.

21. Kato, S., T. Fujimoto and H. Watanabe, *Form Drag Reduction of a Bluff-Based Body with the Aid of Thin Circular-Arc Vanes*, Nippon Kikai Gakkai Ronbunshu, B Hen vol 52, number 480, Aug 1986 pp. 2913-2919.

22. World Meteorological Organization, Technical Note No.59, *Windbreaks and Shelterbelts*, Geneva, Switzerland, 1964.

23. Perera, M.D.A.E.S., *Shelter Behind Two-Dimensional Solid and Porous Fences*, Journal of Wind Engineering and Industrial Aerodynamics, Vol. 8, 1981, pp. 93-104.

24. Gandemer, J., *The Aerodynamic Characteristics of Windbreaks, Resulting on Empirical Design Rules*, Journal of Wind Engineering and Industrial Aerodynamics, Vol. 7, 1981, pp. 15-36.

25. Counihan, J., *An Improved Method of Simulating an Atmospheric Boundary Layer in a Wind Tunnel*, Atmospheric Environment, v. 3, pp. 197-214, 1969.

26. DISA Electronics (Dantec), *DISA Probe Manual*, Denmark, 1982.

27. Anderson, G. A., *Mapping The Airwake Of A Model DD-963 Along Specific Helicopter Flight Paths*, M.S. Thesis, Naval Postgraduate School, Monterey, California, December 1989.

28. Dantec Corporation, *56c17 CTA Fridge Instruction Manual*, Dantec Documentation Department, Denmark, undated.

29. MetraByte Corporation, *Dash-16/16F Manual*, Taunton, Mass., 1986.

30. Murakami, S. and A. Mochida, *3-D Numerical Simulation of Airflow Around a Cubic Model by Means of the Model*, Journal of Wind Engineering and Industrial Aerodynamics, Vol. 31, 1988, pp. 283-303.

31. Yeung, P. and S. Kot, *Computation of Turbulent Flows Past Arbitrary Two-Dimensional Surface-Mounted Obstructions*, Journal of Wind Engineering and Industrial Aerodynamics, Vol. 18, 1985 pp.177-190.

32. Healey, J. V., *Establishing a Database for Flight in the Wakes of Structures*, to be published.

INITIAL DISTRIBUTION LIST

		No. Copies
1.	Defense Technical Information Center Cameron Station Alexandria, Virginia 22304-6145	2
2.	Library, Code 52 Naval Postgraduate School Monterey, California 93943-5002	2
3.	Department Chairman, Code AA/Wo Department of Aeronautics and Astronautics Naval Postgraduate School Monterey, California 93943-5000	1
4.	Commander Naval Air Systems Command Air Vehicle Division Attn: Mr. Jonah Ottensoser, Code Air 53011C Jefferson Plaza 2, Rm. 904 Washington, D.C. 209361	2
5.	Mr. Bernard Ferrier CANDAIR LTD 1800 Laurentieu Blvd. Saint Laurent Quebec, Canada H4R1KZ	1
6.	Naval Air Test Center Attn: Mr. Dean Carico, Code RW40A Patuxent River, Maryland 20670	1
7.	Naval Air Test Center Attn: Mr. Jerry Higman, Code RW81 Patuxent River, Maryland 20670	1

8. Dr. J. Val Healey, Code AA/He — 3
Department of Aeronautics and Astronautics
Naval Postgraduate School
Monterey, California 93943-5000

9. Mr. Neil Gilbert — 1
Aeronautical Division
Aeronautical Research Laboratories
506 Lorimer Street
Fisherman's Bend
Box 4331 P.O.
Melbourne, Victoria 3001
Australia

10 LCDR Marshall Narveson — 1
2212 Burgener Blvd.
San Diego, California 92110